Kernel Metrics on Normal Cycles and Application to Curve Matching

Pierre Roussillon, Joan Alexis Glaunès

KERNEL METRICS ON NORMAL CYCLES AND APPLICATION TO CURVE MATCHING.

PIERRE ROUSSILLON* AND JOAN ALEXIS GLAUNÈS*

October 4, 2016

Abstract. In this work we introduce a new dissimilarity measure for shape registration using the notion of normal cycles, a concept from geometric measure theory which allows to generalize curvature for non smooth subsets of the euclidean space. Our construction is based on the definition of kernel metrics on the space of normal cycles which take explicit expressions in a discrete setting. This approach is closely similar to previous works based on currents and varifolds [32, 12]. We derive the computational setting for discrete curves in $\mathbb{R}^3$, using the Large Deformation Diffeomorphic Metric Mapping framework as model for deformations. We present synthetic and real data experiments and compare with the currents and varifolds approaches.

Key words. Image registration, curve registration, curve matching, normal cycle, geometric measure theory, currents, varifolds, Reproducing Kernel Hilbert Spaces, LDDMM, diffeomorphic models, computational anatomy.

AMS subject classifications. 53C65, 49Q15, 28A75, 37K65, 46E22, 65D18, 62H35, 68U10, 68U05

Introduction. Many applications in medical image analysis require a coherent alignment of images as a pre-processing step, using efficient rigid or non-rigid registration algorithms. Moreover, in the field of computational anatomy, the estimation of optimal deformations between images, or geometric structures segmented from the images, is a building block for any statistical analysis of the anatomical variability of organs. Non-rigid registration is classically tackled down by minimizing a functional composed of two terms, one enforcing regularity of the mapping, and the data-attachment term which evaluates dissimilarity between shapes. Defining good data-attachment terms is important, as it may improve the minimization process, and focuses the registration on the important features of the shapes to be matched.

In [32, 21] a new framework for dissimilarity measures between sub-manifolds was proposed using kernel metrics defined on spaces of *currents*. This setting is now commonly used in computational anatomy ; its advantages lie in its simple implementation and the fact that it provides a common framework for continuous and discrete shapes (see [15] for a computational analysis of currents and their numerical implementation). However, currents are oriented objects and thus a consistent orientation of shapes is needed for a coherent matching. Moreover, due to this orientation property, artificial cancellation can occur with shapes with high local variations. To deal with this problem, a more advanced model based on *varifolds* has been introduced recently [11]. Varifolds are measures over fields of non-oriented linear subspaces. See [11], chap. 3 for an exhaustive analysis.

In this work, we propose to use a second-order model called *normal cycle* for defining shape dissimilarities. The normal cycle of a submanifold X is the current associated with its normal bundle $\mathcal{N}_X$. The normal cycle encodes second order, i.e. curvature information of X; more precisely one can compute integrals of curvatures by evaluating the normal cycle over simple differential forms. Moreover, it has a canonical orientation which is independent of the orientation of X (in fact X does not need to be

*Université Paris Descartes, Sorbonne Paris Cité, MAP5 UMR 8145 (pierre.roussillon@parisdescartes.fr, alexis.glaunes@mi.parisdescartes.fr).

oriented). This is explained by Zähle in [35]: "Although curvature measures describe second order properties of the sets, the first order theory suffices for deriving integral geometric relations. The key is to consider the unit normal bundle of the sets as a locally $(d-1)$-rectifiable subset of $\mathbb{R}^{2d}$ and to observe that the first order infinitesimal behaviour of the unit normal bundle determines the curvature measures." It will be seen in subsection 1.2.3. Our approach is closely related to the currents and varifolds models in that it is based on the definition of kernel metrics that take explicit form in a discrete setting.

This paper is organized as follows. In section 1 we recall definitions and results about currents and normal cycles. Note that in subsection 1.2.5 we derive the action of a diffeomorphism on a normal cycle, which is a new result up to our knowledge. section 2 is devoted to reproducing kernels: the first part (subsections 2.1 and 2.2) recalls known material about kernels in a general setting and in the context of currents. Then is introduced the main idea of our work: the definition of kernel metrics on normal cycles to define data attachment terms for matching problems. This is done in subsection 2.3, where these kernels are defined as products of a spatial and a spherical kernel. We prove embedding result for the Hilbert metric, as well as a universality property of the kernels, which guarantees that we obtain a proper metric on normal cycles (subsection 2.5). In section 3 we investigate the computational aspect of such kernel metrics: we prove convergence result for the Hilbert metric on normal cycles (subsection 3.1, Proposition 31 and Theorem 32), and we propose a computational discrete framework (subsection 3.2) for discrete curves defined as unions of segments, and derive explicit formulas for the metric in the case of discrete curves in $\mathbb{R}^3$. In section 4 we introduce the general curve matching problem, recall some basic facts about the diffeomorphic framework, and prove the existence of minimizers for the corresponding matching problems (Theorem 41 and Proposition 43 in subsection 4.1). Finally in section 5 we show experimental results: two sets of synthetic experiments and an experiment on real data, with the matching of brain sulcal curves.

1. Shapes Representation with Normal Cycles.

1.1. Currents. The concept of currents was first developed as a generalization of distributions, in the sense of Laurent Schwartz. The space of currents can be indeed defined as the topological dual of some space of differential forms. It was later used in geometric measure theory, as it turned out to be a coherent framework for calculus of variations (e.g. Plateau's problem: the existence of an area minimizing surface given a constrained border). Kernel metrics on spaces of currents were proposed and developed in [32, 21, 22] as a way to evaluate the dissimilarity between shapes in computational anatomy. The main advantages of this setting are the ability to represent shapes in a common vectorial space, the existence of straightforward formulae for computing dissimilarities, and the fact that it encompasses both continuous and discrete shapes in the same setting.

We first briefly remind some definitions and results about currents, as it is the fundamental underpinning for normal cycles.

In this paper, $\Lambda^m(\mathbb{R}^d)$ stands for the space of m-vectors in $\mathbb{R}^d$, i.e. the vectorial space generated by the m-simple vectors: $\left\{u_1 \wedge \cdots \wedge u_m,\ u_1, \ldots, u_m \in \mathbb{R}^d\right\}$. This is an euclidean space, with the canonical scalar product on m-simple vectors (denoted $\langle ., . \rangle_{\Lambda^m(\mathbb{R}^d)}$ or simply $\langle ., . \rangle$ when there is no ambiguity)

$$\langle u_1 \wedge \cdots \wedge u_m, v_1 \wedge \cdots \wedge v_m \rangle = \det\left((u_i \cdot v_j)_{1 \leq i,j \leq m}\right)$$

where $x \cdot y$ is the canonical scalar product on $\mathbb{R}^d$. The norm associated with this

scalar product in $\Lambda^m(\mathbb{R}^d)$ is denoted $|.|_{\Lambda^m(\mathbb{R}^d)}$ or $|.|$. We also denote the dual pairing between $w \in (\Lambda^m(\mathbb{R}^d))^*$, the dual of $\Lambda^m(\mathbb{R}^d)$ and $u \in \Lambda^m(\mathbb{R}^d)$: $\langle w|u\rangle := w(u)$. Via the Riesz representation theorem, we can associate to w a unique m-vector $\overline{w}$ such that $\forall u \in \Lambda^m(\mathbb{R}^d), \langle w|u\rangle = \langle \overline{w}, u\rangle$.

For the definition of currents used in this paper, we consider the space of continuous m-differential forms vanishing at infinity $\Omega_0^m(\mathbb{R}^d) := \mathcal{C}_0^0(\mathbb{R}^d, (\Lambda^m\mathbb{R}^d)^*)$, with the norm: $\|\omega\|_\infty = \sup_{x\in\mathbb{R}^d} |\omega(x)|$. For later use, we also define $\Omega_{k,0}^m(\mathbb{R}^d) := \mathcal{C}_k^0(\mathbb{R}^d, (\Lambda^m\mathbb{R}^d)^*)$ the space of m-differential forms of class C^k, with partial derivatives up to order k vanishing at infinity. We now give the definition of current that we will use in this paper.

Definition 1 (Currents). *The space of m-currents in $\mathbb{R}^d$ is defined as the topological dual of $\Omega_0^m(\mathbb{R}^d)$: $\Omega_0^m(\mathbb{R}^d)'$. $T \in \Omega_0^m(\mathbb{R}^d)'$ maps every differential form ω to $T(\omega) \in \mathbb{R}$ and*

$$T(\omega) \leq C_T \|\omega\|_\infty$$

Example 2. A fundamental example of current (which will be useful when dealing with discrete shapes) is the "Dirac" current. Let $x \in \mathbb{R}^d$, $\alpha \in \Lambda^m(\mathbb{R}^d)$. For $\omega \in \Omega_0^m(\mathbb{R}^d)$, we define $\delta_x^\alpha(\omega) := \langle \omega(x)|\alpha\rangle$.

As we will see right below, using the theory of integration for differential forms, any sufficiently regular shape in $\mathbb{R}^d$ can be seen as a current. In this way, shapes are represented in the vectorial space of currents.

We recall that $\mathcal{H}^m$ is the m-dimensional Hausdorff measure and that in $\mathbb{R}^d$, $\mathcal{H}^d = \lambda^d$ where λ^d is the classical Lebesgue's measure of $\mathbb{R}^d$. Besides, for X a m-dimensional submanifold, $\mathcal{H}^m$ coincides on X with the volume form of X.

First we consider the case of a compact, m-dimensional, oriented $\mathcal{C}^1$-submanifold X on $\mathbb{R}^d$. One can associate to X a current $[X]$ defined as follows:

$$[X](\omega) := \int_X \langle \omega(x)|\tau_X(x)\rangle \, d\mathcal{H}^m(x) \tag{1}$$

where $\tau_X(x) = \tau_1(x)\wedge\cdots\wedge\tau_m(x)$, with $(\tau_i(x))_{1\leq i\leq m}$ a positively oriented, orthonormal basis of T_xX. If $\tilde{X}$ denotes the same submanifold X with opposite orientation, we have $[\tilde{X}] = -[X]$.

In fact, $\mathcal{C}^1$ regularity is too strong for our framework and we will consider *m-rectifiable sets*, which are basically sets defined via Lipschitzian maps ([17], 3.2.14)

Definition 3 (m-rectifiable sets). *A set X of $\mathbb{R}^d$ is said* m-rectifiable *if there exists $(U_i)_{i\in\mathbb{N}}$ a sequence of bounded sets of $\mathbb{R}^m$ and $(f_i)_{i\in\mathbb{N}}$ a sequence of Lipschitz functions $f_i : U_i \to \mathbb{R}^d$ such that $\mathcal{H}^m\left(X \setminus \cup_{i\in\mathbb{N}} f(U_i)\right) = 0$*

Remark 4. In the references, this definition corresponds to the notion of *countably rectifiable set*, but authors usually mean countably rectifiable when they write rectifiable.

Remark 5. There is an equivalent definition due to Federer ([17], 3.2.29): a set X is m-rectifiable if and only if $\mathcal{H}^m$-almost all of X is contained in a countable union of m-dimensional, $\mathcal{C}^1$-submanifolds.

If X is a compact, m-rectifiable set, we can consider for $\mathcal{H}^m$-almost every $x \in X$ the tangent space of X at x, T_xX ([17], 3.2.16 and 3.2.19), and an *orientation* of X will be simply an orientation $o_x \in \{-1, 1\}$ of every tangent space T_xX such that the

application $x \mapsto (T_x X, o_x)$ is $\mathcal{H}^m$ measurable on X. Therefore, we can associate a current $[X]$ to any m-rectifiable set X as in equation (1).

As mentioned and studied in [12], the *orientation*, inherent in the concept of currents is a challenging issue in computational anatomy. Hence, any matching problem between two shapes requires first of all a coherent orientation for both shapes. Assigning coherent orientations between corresponding shapes can be difficult or even arbitrary in some practical applications. More importantly, when using kernel metrics on the space of currents, this orientation issue can lead to artificial cancellation in the space of currents. A high spatial variation of the shape (compared to the typical size of the kernel used for the kernel metric) will not be seen by the metric, due to the orientation. To overcome this problem, Nicolas Charon proposed a model based on *varifolds* [12]. A varifold can be heuristically seen as an *unoriented* distribution of measures with support in the set of all tangent spaces of the shape. In this work, we propose a model based on normal cycles, which are currents associated to the unit normal bundle. As we will see it does not require any orientation of the shape itself, and shares some similarities with the approach based on varifolds. Although the mathematical frameworks are different, the normal cycles metrics we will introduce can be seen in some sense as extensions of metrics based on varifolds.

1.2. Normal cycles. Normal cycles find their roots in the seminal work of Federer. In [16], he proved that for a set with positive reach X (see definition below), the volume of the ε-parallel neighbour of $X \cap B$ (where B is a borelian) can be expressed as a polynomial of ε, and more importantly that the coefficients of this polynomial can be interpreted as *curvature measures* of the set X. These measures have integral representation, and Zähle in [35] introduced $(d-1)$-generalized principal curvatures for sets with positive reach, and retrieved Federer's curvature measures by integrating functions of these principal curvatures over the unit normal bundle. She showed that it can be done by integrating adequate differential forms on the associated rectifiable current: this is exactly the normal cycle. This work was pushed forward in [36]. A more intrinsic definition of normal cycle can be found in [19], however we will not need such a generalization for our purpose. The book of Morvan ([27]) is a self-sufficient reference for normal cycle as it will be used in this paper.

Normal cycles have already been applied to computational analysis of discrete surfaces in [14]. Cohen-Steiner and Morvan derived a definition of discrete curvature and discrete curvature tensor for polyhedral surfaces using normal cycle. Thus, they could retrieve direction of minimal curvatures for discrete surfaces, and obtained an estimation of the error of the curvature between the approximated surface and the smooth one. In [13], the authors use normal cycles to define curvature measures for point cloud. They compute mean and Gaussian curvatures on the offset of a point cloud sampled around a smooth or non smooth surfaces and retrieve the interesting curvature features of the original continuous surface

We will not investigate more about curvature approximations here, but rather introduce all the tools necessary for normal cycles in a pure geometric measure theory viewpoint. In section 2, kernel metrics will be developed in order to have explicit distance between shapes with normal cycles representation.

1.2.1. Sets of positive reach. The first step is to define a proper framework to consider shapes. For currents and varifolds for example, this framework is the one of m-rectifiable sets. Here, as we want to define a normal bundle associated with the shape, we will need a slightly different framework. As previously said, the normal cycle of a $\mathcal{C}^2$-submanifold X in $\mathbb{R}^d$ is the current associated with its unit normal

bundle $\mathcal{N}_X = \{(x,n) \in \mathbb{R}^d \times S^{d-1} | x \in X, n \in (T_x X)^\perp \cap S^{d-1}\}$. However, the $\mathcal{C}^2$ setting is not the most convenient one to deal with normal cycles. When generalizing the tube formula for convex sets (Steiner's formula) and for $\mathcal{C}^2$-submanifold (Weyl's formula), Federer introduced the notion of sets with *positive reach* ([16], sect. 4), which encompasses both cases. The reach of a set $X \subset \mathbb{R}^d$ is closely linked to the uniqueness of projection on this set for sufficiently close points.

DEFINITION 6 (Reach). *For $\varepsilon > 0$, we define $X_\varepsilon = \{x \in \mathbb{R}^d | d(x,X) \leq \varepsilon\}$ and $\partial X_\varepsilon = \{x \in \mathbb{R}^d | d(x,X) = \varepsilon\}$. The reach of X, denoted reach(X), is the supremum of real numbers $\varepsilon > 0$ such that there exists a unique projection of any $x \in X_\varepsilon$ onto X. X is said to be a* positive reach set *if reach$(X) > 0$. If $0 < \varepsilon < reach(X)$, we denote $P_X : X_\varepsilon \to X$ the projection application.*

PR is the class of sets with positive reach.

Remark 7. If X is convex, $\mathrm{Reach}(X) = +\infty$. If X is a compact $\mathcal{C}^2$-submanifold, X has a positive reach.

On a set with positive reach R, we can roll a ball of radius less than R. Thus, a set with positive reach can be seen heuristically as a set with a bounded below curvature.

DEFINITION 8 (Tangent Bundle and Unit Normal bundle). *Let X be a set with positive reach.*

1. The tangent cone of X at point x *is*

$$\mathrm{Tan}(X,x) := \left\{v \in \mathbb{R}^d, \forall \varepsilon > 0, \exists y \in X, \exists c > 0, |x-y| < \varepsilon \text{ and } |c(y-x) - v| < \varepsilon\right\}$$

It is a closed cone ([16]).

2. $\mathcal{T}_X := \{(x,v) : x \in X, v \in \mathrm{Tan}(X,x)\}$ is the tangent bundle of X.

3. The normal cone of X at point x *is defined as the polar cone of* $\mathrm{Tan}(X,x)$*:*

$$\mathrm{Nor}(X,x) := \left\{u \in \mathbb{R}^d, \forall v \in \mathrm{Tan}(X,x), \langle u, v\rangle \leq 0\right\}$$

$\mathrm{Nor}(X,x)$ *is a closed convex cone.*

4. The set of unit normal vectors *is defined as* $\mathrm{Nor}^u(X,x) := \mathrm{Nor}(X,x) \cap S^{d-1}$.

5. $\mathcal{N}_X = \{(x,n) \in (\mathbb{R}^d)^2, x \in X, n \in \mathrm{Nor}^u(X,x)\}$ is the unit normal bundle of X.

Remark 9. For a $\mathcal{C}^2$-submanifold, the unit normal bundle defined here coincides with the classical one, which is a $(d-1)$-submanifold in the $(2d-1)$ dimensional space $\mathbb{R}^d \times S^{d-1}$.

Remark 10. If $x \in \mathring{X}$, the interior of X, then $\mathrm{Tan}(X,x) = \mathbb{R}^d$ and consequently $\mathrm{Nor}^u(X,x) = \emptyset$.

Example 11 (Unit normal bundle of a curve in $\mathbb{R}^d$). We give here the description of the normal bundle associated to a regular curve in $\mathbb{R}^d$. Let $\gamma : [0,L] \to \mathbb{R}^d$ be the parametrization of a C^1 regular non-intersecting and non-closed curve C in $\mathbb{R}^d$. On a regular point along the curve (i.e. $\gamma(t)$, $0 < t < L$), one has $\mathrm{Nor}^u(C,\gamma(t)) = \gamma'(t)^\perp \cap S^{d-1}$. For the singular part (i.e. the two endpoints), we denote $S_v^+ := \{u \in S^{d-1} \mid \langle u, v\rangle \geq 0\}$. One can easily show that $\mathrm{Nor}^u(C,\gamma(0)) = S^+_{-\gamma'(0)}$ and $\mathrm{Nor}^u(C,\gamma(1)) = S^+_{\gamma'(1)}$. These are two half spheres with a coherent orientation with respect to the normal bundle (independent of the parametrization). See Figure 1 for an illustration.

The generalized normal bundle $\mathcal{N}_X$ is a subset of $\mathbb{R}^d \times S^{d-1} \subset \mathbb{R}^d \times \mathbb{R}^d$, and since X is a set with positive reach, we can visualize $\mathcal{N}_X$ in $\mathbb{R}^d$: choose $0 < \varepsilon < \mathrm{Reach}(X)$ and consider the application

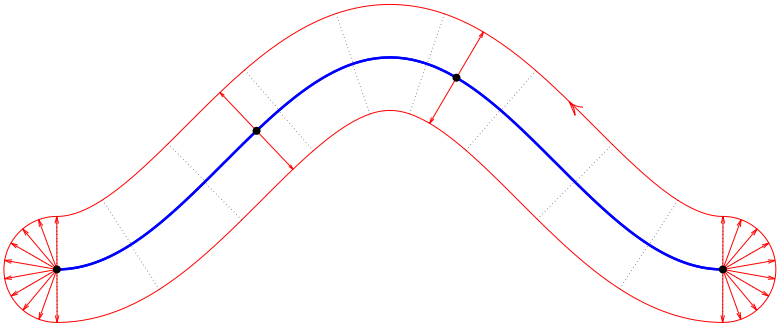

FIG. 1. *Illustration of the unit normal bundle for a regular non closed curve in the plane. The curve is in blue, the unit normal vectors associated to four points are represented as red arrows, and the resulting unit normal bundle is represented in red, with its canonical orientation. Note that this representation is only illustrative, as the true normal bundle belongs to the space* $\mathbb{R}^2 \times S^1$ *in this case*

$$(x, n) \in \mathcal{N}_X \mapsto x + \varepsilon n \in \mathbb{R}^d \tag{2}$$

Thus, the normal bundle can be depicted in $\mathbb{R}^d$, using (2) by considering the ε-tube around the set X.

Even if the definition of positive reach relies on few hypotheses, a set with positive reach has remarkable regularity properties:

PROPOSITION 12. *Let* X *be a set with positive reach* $R > 0$*, and* $0 < \varepsilon < R$*.* ∂X_ε *is a* $\mathcal{C}^1$*-hypersurface (a* $(d-1)$*-dimensional,* $\mathcal{C}^1$*-submanifold in* $\mathbb{R}^d$*), with Lipschitzian normal vector field.*

Proof. We summarize here the main results of [16], 4.8. On X_ε, the projection P_X is well defined. Moreover, if we denote $\delta(x) = d(x, X)$ for every $x \in X_r$, we can rewrite: $\partial X_\varepsilon = \{x \in \mathbb{R}^d | \delta(x) = \varepsilon\}$. 4.8. (5) of [16] guarantees that δ is continuously differentiable on the interior of $X_\varepsilon \setminus X$, with $\nabla\delta(x) = \frac{x - P_X(x)}{\delta(x)}$. Thus, ∂X_ε is defined as an implicit $\mathcal{C}^1$ real valued function, with non null differential, and therefore is an hypersurface.

Moreover, one can show that the outward unit normal vector of ∂X_ε at point x is given by $n(x) = \frac{x - P_X(x)}{\delta(x)} = \nabla\delta(x)$. And 4.8 (9) of [16] states that $\nabla\delta$ is Lipschitzian on ∂X_ε. Thus, ∂X_ε has Lipschitzian normal vector field. ∎

The next proposition draws a more precise link between ∂X_ε and the normal bundle $\mathcal{N}_X$.

PROPOSITION 13. *Let* X *be a set with positive reach,* $0 < \varepsilon < Reach(X)$ *and* P_X *be the projection on* X*, which is well defined on* X_ε*. Then*

$$\varphi_\varepsilon : \partial X_\varepsilon \to \mathcal{N}_X : y \mapsto \left(P_X(y), \frac{y - P_X(y)}{\varepsilon} \right)$$

is bijective and bi-Lipschitz, with inverse mapping

$$g_\varepsilon : \mathcal{N}_X \to \partial X_\varepsilon : (x, n) \mapsto x + \varepsilon n$$

This proposition is the key argument to obtain the next theorem, which is fundamental to define normal cycles.

THEOREM 14. *If X is a set with positive reach, $\mathcal{N}_X$ is a $(d-1)$-rectifiable set in $\mathbb{R}^d \times \mathbb{R}^d$.*

Proof. This is just an application of Proposition 13 with Proposition 12, and by using the definition of rectifiability seen above: $\mathcal{N}_X$ is the image of the Lipschitzian map g_ε of the $\mathcal{C}^1$ submanifold ∂X_ε. ∎

Thus, with a set with positive reach, one can associate the current of its $(d-1)$-rectifiable unit normal bundle.

Orientation of $\mathcal{N}_X$. A last aspect to precise is the orientation. We recall that a current is an oriented object, hence to define the current associated with the normal bundle, the normal bundle needs to be oriented. Again, a nice property of a set with positive reach is that its normal bundle has a canonical orientation which does not require the set itself to be oriented. From now on, we denote by π_0 the projection on the spatial space, and π_1 the projection on the normal space: $\pi_0 : (x,n) \in \mathbb{R}^d \times S^{d-1} \mapsto x$, $\pi_1 : (x,n) \in \mathbb{R}^d \times S^{d-1} \mapsto n$. One should note that *the unit normal bundle has a canonical orientation* arising from the orientation of ∂X_ε as follows: let $(e_1, \dots, e_d)$ be the standard basis of $\mathbb{R}^d$, and $(a_1(x,n), \dots, a_{d-1}(x,n))$ an orthonormal basis of $T_{(x,n)}\mathcal{N}_X$ (which is well defined $\mathcal{H}^{d-1}$-almost everywhere on $\mathcal{N}_X$). We say that $(a_1(x,n), \dots, a_{d-1}(x,n))$ is positively oriented if

$$\langle ((\pi_0 + \varepsilon\pi_1)(a_1(x,n)) \wedge \cdots \wedge (\pi_0 + \varepsilon\pi_1)(a_{d-1}(x,n)) \wedge n, e_1 \wedge \cdots \wedge e_d \rangle > 0. \tag{3}$$

This quantity is independent of $0 < \varepsilon < \mathrm{Reach} X$ [35]. Then $a(x,n) = a_1(x,n) \wedge \cdots \wedge a_{d-1}(x,n)$ fulfilling (3) (independent of the choice of the orthonormal basis verifying the last hypothesis) may be considered as a $(d-1)$-vectorfield orienting $\mathcal{N}_X$.

1.2.2. Normal Cycle. Since $\mathcal{N}_X$ is an orientable rectifiable set of $\mathbb{R}^d \times \mathbb{R}^d$ (independently of any orientation of X), we can consider its current, an element of $\Omega_0^{d-1}(\mathbb{R}^d \times \mathbb{R}^d)'$, which is called the normal cycle. For later considerations with reproducing kernels, we introduce also the space $\Omega_0^{d-1}(\mathbb{R}^d \times S^{d-1}) = \mathcal{C}_0^0(\mathbb{R}^d \times S^{d-1}, \Lambda^{d-1}(\mathbb{R}^d \times \mathbb{R}^d)^*)$ and its topological dual $\Omega_0^{d-1}(\mathbb{R}^d \times S^{d-1})'$. Since integration of a differential form ω over $\mathcal{N}_X$ only depends on the values of ω in $\mathbb{R}^d \times S^{d-1}$, it is equivalent to consider the normal cycle as an element of $\Omega_0^{d-1}(\mathbb{R}^d \times \mathbb{R}^d)'$ or $\Omega_0^{d-1}(\mathbb{R}^d \times S^{d-1})'$.

DEFINITION 15 (Normal cycle). *The normal cycle of a set X with positive reach is the $(d-1)$-current associated to $\mathcal{N}_X$. If $\omega \in \Omega_0^{d-1}(\mathbb{R}^d \times S^{d-1})$ is a $(d-1)$-differential form on $\mathbb{R}^d \times S^{d-1}$, one has*

$$N(X)(\omega) := [\mathcal{N}_X](\omega) = \int_{\mathcal{N}_X} \langle \omega(x,n) | \tau_{\mathcal{N}_X}(x,n) \rangle \, d\mathcal{H}^{d-1}(x,n) \tag{4}$$

where $\tau_{\mathcal{N}_X}(x,n)$ is the $(d-1)$-vector associated with an orthonormal positively oriented basis of $T_{(x,n)}\mathcal{N}_X$. For any Borel subset $B \subset \mathbb{R}^d \times S^{d-1}$, we also define the restricted current $N(X) \llcorner \mathbb{1}_B$:

$$N(X) \llcorner \mathbb{1}_B(\omega) := N(X)(\omega \mathbb{1}_B) \tag{5}$$

Remark 16. In the previous definition of the restriction of $N(X)$, $\omega \mathbb{1}_B$ is not necessarily continuous, which might seem as a problem given the definition of a normal cycle. However, as explained in [17], 4.1.7, since $N(X)$ is representable by integration (here it is canonically associated with the rectifiable set $\mathcal{N}_X$), it is sufficient for the differential form to be integrable over $\mathcal{N}_X$.

Hence, the normal cycle is a tool to canonically represent a set with positive reach.

1.2.3. Lipschitz-Killing curvatures and normal cycle. Here we formalize more specifically the link between the normal cycle of a set X with positive reach, and its curvatures. For this purpose, we define some *invariant, universal differential forms* on $\mathbb{R}^d \times S^{d-1}$, the Lipschitz-Killing forms.

Let $(x, n) \in \mathbb{R}^d \times S^{d-1}$. We set $e_1(x, n)$, ..., $e_{d-1}(x, n) \in \mathbb{R}^d$ such that $(e_1(x, n)$, ..., $e_{d-1}(x, n), n)$ is an orthonormal basis of $\mathbb{R}^d$, and we denote

$$\varepsilon_1 = \begin{pmatrix} e_1 \\ 0 \end{pmatrix}, \ldots, \varepsilon_d = \begin{pmatrix} n \\ 0 \end{pmatrix}$$
$$\tilde{\varepsilon}_1 = \begin{pmatrix} 0 \\ e_1 \end{pmatrix}, \ldots, \tilde{\varepsilon}_{d-1} = \begin{pmatrix} 0 \\ e_{d-1} \end{pmatrix}$$

where we omit the dependency on (x, n). This enables us to define a polynomial in the real variable t:

$$\nu(t) = (\varepsilon_1 + t\tilde{\varepsilon}_1) \wedge \cdots \wedge (\varepsilon_{d-1} + t\tilde{\varepsilon}_{d-1})$$

which is a $(d-1)$-vector field in $\mathbb{R}^d \times S^{d-1}$. Even though the $(e_i)_{1 \leq i \leq d-1}$ are not uniquely defined (an orthonormal change of basis is still a valid candidate), the expression of ν is independent of the choice of this orthonormal basis, and thus is well defined.

For $0 \leq k \leq d-1$, we denote ν_k the coefficient of the monomial t^{d-k-1} of ν, and define the $(d-1)$-form $\boldsymbol{\omega}_k$ which is canonically identified to the (d-1)-vector field

$$\overline{\boldsymbol{\omega}}_k := \frac{\nu_k}{(d-k)\alpha_{d-k}}$$

where α_k is the volume of the k-dimensional unit ball.

Definition 17 (Lipschitz-Killing forms). *$\boldsymbol{\omega}_k$, $0 \leq k \leq d-1$ is called the k^{th} Lipschitz-Killing form. The Lipschitz-Killing forms are euclidean motion invariants (see [27], Chap. 19).*

We can sum up the announced results of Federer and Zähle on these curvature measures in a theorem (see [16, 35, 36])

Theorem 18. *If X is a set with positive reach $R > 0$ and $\varepsilon < R$, we have*

$$\mathrm{Vol}\left((X \cap B)_\varepsilon\right) = \sum_{k=0}^{d} \alpha_k C_{d-k}(X; B)\varepsilon^k \tag{6}$$

where $C_k(X; B) = N(X) \llcorner \mathbb{1}_{B \times S^{d-1}}(\boldsymbol{\omega}_k)$, for $0 \leq k \leq d-1$ and $C_d(X; B) := \mathcal{H}^d(X \cap B)$.

It can be shown, as detailed in [5], that these $C_k(X; .)$ coincide with the classical definition of curvatures for $\mathcal{C}^2$ hypersurfaces. In the case of an oriented m-dimensional

submanifold X of $\mathbb{R}^d$ without boundary, one has (see [27], chap. 21)

$$C_i(X;\cdot) = 0, \;\; m < i \leq d$$

which means that the first coefficients of the polynomial (6) are null. Moreover, $C_m(X;B) = \mathcal{H}^m(X \cap B)$ and $C_{m-2}(X;B) = \int_{X\cap B} s(x) d\mathcal{H}^m(x)$ up to a constant, where $s(x)$ is the scalar curvature of X at x. The next proposition justifies the designation of curvature measures.

PROPOSITION 19. *The $C_k(X;.)$ are euclidean motion invariant, signed Radon measures. Moreover, they are additive: if X, Y, $X \cup Y$ and $X \cap Y$ have positive reach, then*

$$C_k(X \cup Y;\cdot) = C_k(X;\cdot) + C_k(Y;\cdot) - C_k(X \cap Y;\cdot)$$

To make the connection with the usual notion of curvature in differential geometry, let us derive the expression of the normal cycle in the simple case of a non-self intersecting regular closed curve C in $\mathbb{R}^2$ with $\mathcal{C}^2$ regularity. Let $\gamma : [0, L] \to \mathbb{R}^2$ be an arc-length parametrization of C, with L its length. We denote $\tau(s) = \gamma'(s)$ the unit tangent vector and $n(s) = \tau(s)^\perp$ the unit normal vector such that $(\tau(s), n(s))$ is positively oriented. The scalar curvature $\kappa(s)$ is defined via the formula $n'(s) = \kappa(s)\tau(s)$. At each point $x = \gamma(s)$ of the curve, there are two unitary normal vectors $n(s)$ and $-n(s)$, so that the unit normal bundle $\mathcal{N}_C$ is composed of two disconnected curves with parametrizations $\Gamma_1(s) = (\gamma(s), n(s))$ and $\Gamma_2(s) = (\gamma(L-s), -n(L-s))$ (taking into account the canonical orientation of $\mathcal{N}_C$). The expression of the normal cycle over a 1-form ω thus writes

$$N(C)(\omega) = N(C)_1(\omega) + N(C)_2(\omega)$$

with

$$N(C)_1(\omega) := \int_0^L \langle \omega(\Gamma_1(s)) | \Gamma_1'(s) \rangle \, ds, \quad N(C)_2(\omega) := \int_0^L \langle \omega(\Gamma_2(s)) | \Gamma_2'(s) \rangle \, ds.$$

The 1-form ω can be identified to a vector-field $\bar{\omega}$ on $T(\mathbb{R}^2 \times S^1)$ written in the form

$$\bar{\omega}(x, n) = (\bar{\omega}_p(x, n), \bar{\omega}_n(x, n) e_1),$$

where $\bar{\omega}_p(x, n) \in \mathbb{R}^2$, $\bar{\omega}_n(x, n) \in \mathbb{R}$ and, as defined previously, e_1 the unitary vector such that (e_1, n) is a positively oriented basis of $\mathbb{R}^2$. With these notations one gets after computations

$$N(C)_1(\omega) = \int_0^L \langle \bar{\omega}_p(\gamma(s), n(s)), \tau(s) \rangle \, ds + \int_0^L \bar{\omega}_n(\gamma(s), n(s)) \kappa(s) ds,$$

and

$$N(C)_2(\omega) = -\int_0^L \langle \bar{\omega}_p(\gamma(s), -n(s)), \tau(s) \rangle \, ds - \int_0^L \bar{\omega}_n(\gamma(s), -n(s)) \kappa(s) ds.$$

This shows clearly the link between the normal cycle and curvature in this case. For example it is clear from these expressions that one has

$$\sup \left\{ N(C)(\omega), \omega \in \Omega_0^1(\mathbb{R}^2 \times S^1), \|\omega\|_\infty \leq 1 \right\} = 2L + 2 \int_0^L |\kappa(s)| ds,$$

and further one gets the length and the integral of the absolute value of the curvature as

$$L = \frac{1}{2}\sup\left\{N(C)(\omega), \omega \in \Omega_0^1(\mathbb{R}^2 \times S^1), \|\omega\|_\infty \leq 1, \bar{\omega}_n = 0\right\} = N(C)(\boldsymbol{\omega}_1),$$

$$\int_0^L |\kappa(s)|ds = \frac{1}{2}\sup\left\{N(C)(\omega), \omega \in \Omega_0^1(\mathbb{R}^2 \times S^1), \|\omega\|_\infty \leq 1, \bar{\omega}_p = 0\right\},$$

which can be also localized: for any Borel subset $B \in \mathbb{R}^2$,

$$\begin{aligned}\mathcal{H}^1(C \cap B) &= N(C)\llcorner \mathbb{1}_{B\times S^{d-1}}(\boldsymbol{\omega}_1)\\ \int_{\gamma^{-1}(C\cap B)} |\kappa(s)|ds &= \frac{1}{2}\sup\left\{N(C)(\omega), \omega \in \Omega_0^1(\mathbb{R}^2 \times S^1),\right.\\ &\qquad \left.\|\omega\|_\infty \leq 1, \bar{\omega}_p = 0, \forall x \in \mathbb{R}^2 \setminus B, \omega(x,n) = 0\right\}.\end{aligned}$$

This clearly shows that curvature is encoded in the normal cycle representation of the curve. However, applying $N(C)$ to the Lipschitz-Killing form $\boldsymbol{\omega}_0$ gives the following (since $\boldsymbol{\omega}_0 = \tilde{\varepsilon}_1 = (0, e_1)$):

$$N(C)_1(\boldsymbol{\omega}_0) = \int_0^L \kappa(s)ds, \quad N(C)_2(\boldsymbol{\omega}_0) = -\int_0^L \kappa(s)ds,$$

so that $N(C)(\boldsymbol{\omega}_0) = 0$. In fact the sign of the scalar curvature depends on the choice of orientation of the curve, whereas the normal cycle does not encode orientation. Thus it is normal that one cannot hope to retrieve the integral of the signed curvature from the full expression of the normal cycle. The non trivial application of theorem 18 in this case appears when considering the normal cycle of the compact domain $V \subset \mathbb{R}^2$ such that $\partial V = C$ (which exists via Jordan's theorem). It can be easily seen that $N(V) = N(C)_1$, so that the curvature measure $C_1(V, \cdot)$ corresponds to the integral of κ:

$$C_0(V; B) = \int_{\gamma^{-1}(C\cap B)} \kappa(s)ds.$$

In general however, when considering non closed curves in $\mathbb{R}^2$ or curves in $\mathbb{R}^3$, C does not correspond to the boundary of any domain, and there is no way to get rid of the cancelling effect. In fact, it can be shown that C_{m-i} vanishes for i odd, in the case of a m submanifold of $\mathbb{R}^d$. But one should not misinterpret this point: it only means that the Lipschitz-Killing forms and the curvature measures are not the right tool in this context ; the normal cycle itself still encodes all curvature information.

We now specify Theorem 18 in the case of a regular surface in $\mathbb{R}^3$. The Lipschitz-Killing 2-differential forms on $\mathbb{R}^3$ are

$$\boldsymbol{\omega}_0 = \frac{\tilde{\varepsilon}_1 \wedge \tilde{\varepsilon}_2}{4\pi}, \ \boldsymbol{\omega}_1 = \frac{\tilde{\varepsilon}_1 \wedge \varepsilon_2 + \varepsilon_1 \wedge \tilde{\varepsilon}_2}{4\pi}, \ \boldsymbol{\omega}_2 = \frac{\varepsilon_1 \wedge \varepsilon_2}{2}$$

where we keep the same notations as in Definition 17. For the sake of simplicity, we will consider a domain M of $\mathbb{R}^3$ (i.e. a submanifold of dimension 3), with boundary $S = \partial M$. S is an orientable surface, with outward normal vector field n.

One can show that the application

$$\varphi : S \to \mathcal{N}_M \cap (S \times S^{d-1}), x \mapsto (x, n(x))$$

is a diffeomorphism, and using Note 10, it can be shown that $C_k(M, B) = C_k(M, B \cap \mathrm{Bdry}(M))$ where $\mathrm{Bdry}(M) = \overline{M} \setminus \mathring{M}$. (here $\mathrm{Bdry}(M) = \partial M = S$). We have

$$\begin{aligned} C_k(M; B) &= N(M) \llcorner \mathbb{1}_{B \times S^{d-1}}(\boldsymbol{\omega}_k) \\ &= N(S) \llcorner \mathbb{1}_{B \times S^{d-1}}(\boldsymbol{\omega}_k) \end{aligned}$$

and thus

$$\begin{aligned} N(M) \llcorner \mathbb{1}_{B \times S^{d-1}}(\boldsymbol{\omega}_1) &= \int_{\mathcal{N}_M \cap (B \times S^{d-1})} \boldsymbol{\omega}_1 = \int_{\varphi(S \cap B)} \boldsymbol{\omega}_1 \\ &= \int_{S \cap B} \langle \boldsymbol{\omega}_1(\varphi(x)) | d\varphi_u(b_1(x)) \wedge d\varphi_u(b_2(x)) \rangle \, d\mathcal{H}^2(x, n) \end{aligned}$$

where the last row is obtained by a change of variable for differential forms. Since $d\varphi_u = \begin{pmatrix} \mathrm{Id}_{\mathbb{R}^3} & dn_x \end{pmatrix}$ (where the b_i appearing in this theorem are the eigenvectors of dn_x), we get:

$$\begin{aligned} N(M) \llcorner \mathbb{1}_{B \times S^{d-1}}(\boldsymbol{\omega}_1) &= \frac{1}{4\pi} \int_{S \cap B} \left\langle \begin{pmatrix} 0 \\ b_1 \end{pmatrix} \wedge \begin{pmatrix} b_2 \\ 0 \end{pmatrix} \middle| \begin{pmatrix} b_1 \\ k_1 b_1 \end{pmatrix} \wedge \begin{pmatrix} b_2 \\ k_2 b_2 \end{pmatrix} \right\rangle \\ &+ \frac{1}{4\pi} \int_{S \cap B} \left\langle \begin{pmatrix} b_1 \\ 0 \end{pmatrix} \wedge \begin{pmatrix} 0 \\ b_2 \end{pmatrix} \middle| \begin{pmatrix} b_1 \\ k_1 b_1 \end{pmatrix} \wedge \begin{pmatrix} b_2 \\ k_2 b_2 \end{pmatrix} \right\rangle \\ &= \frac{1}{4\pi} \int_{S \cap B} (k_1(x) + k_2(x)) d\mathcal{H}^2(x) = C_1(S; B) \end{aligned}$$

We retrieve the mean curvature measure of S thanks to the normal cycle of M. With the same calculation, we obtain:

$$N(M) \llcorner \mathbb{1}_{B \times S^{d-1}}(\boldsymbol{\omega}_0) = \frac{1}{4\pi} \int_{S \cap B} k_1(x) k_2(x) d\mathcal{H}^2(x)$$

which is the Gauss curvature measure on S up to a constant, and

$$N(X) \llcorner \mathbb{1}_{B \times S^{d-1}}(\boldsymbol{\omega}_2) = \frac{1}{2} \int_{S \cap B} d\mathcal{H}^2(x) = \frac{1}{2} \mathcal{H}^2(S \cap B)$$

which is the area measure on S up to a constant.

1.2.4. Unions of Sets with Positive Reach. We have seen here how to represent some shapes with normal cycles: $\mathcal{C}^2$ compact submanifolds and convex sets for example are sets with positive reach and have such a representation. However polyhedral approximations of curves and surfaces do not have positive reach anymore, and these are the objects we will consider to derive practical algorithms. But fortunately the theory of normal cycles can be extended to a class of sets containing unions of sets with positive reach, as developed in [36, 29, 31]. We briefly introduce this extension here, referring to these works for all details. The $\mathcal{U}_{PR}$ class is defined as the class of sets X which can be written as a locally finite union of sets X_i, $i \in \mathbb{N}$, such that for any finite subset of indices $I \subset \mathbb{N}$, $\cap_{i \in I} X_i$ is of positive reach. In particular sets of positive reach belong of course to this class, and it contains also all finite unions of non-empty closed convex sets. The normal cycle $N(X)$ associated to a set $X \in \mathcal{U}_{PR}$ can be defined in a recursive way so that the following fundamental additive property is satisfied:

DEFINITION 20 (Additive property). *Assume that sets X, Y, $X \cap Y$ are with positive reach. Then we define*

$$N(X \cup Y) := N(X) + N(Y) - N(X \cap Y) \tag{7}$$

In the case where $X \cup Y$ is with positive reach, this definition is coherent : the left hand side and the right hand side in the definition are equal. In the case of a finite union of sets with positive reach: $X = \cup_{i=1}^{n} X_i$, belonging to $\mathcal{U}_{PR}$, it is easy to see that any combination of unions and intersections of the X_i also belongs to $\mathcal{U}_{PR}$. Hence the additive formula allows to write a recursive expression for the normal cycle of X, which can serve as a definition for normal cycle in this case: for $1 \leq k \leq n$, one has

$$N(X_1 \cup \cdots \cup X_k) = N(X_1 \cup \cdots \cup X_{k-1}) + N(X_k) - N((X_1 \cup \cdots \cup X_{k-1}) \cap X_k)$$

It is possible to define normal cycles in a more intrinsic way (see [29]), using the index function: for a closed subset $X \subset \mathbb{R}^d$, $x \in \mathbb{R}^d$ and $n \in S^{d-1}$, we define:

$$i_X(x,n) = \mathbb{1}_X(x) \left(1 - \lim_{\varepsilon \to 0} \lim_{\delta \to 0} \chi\big(X \cap B(x + (\varepsilon + \delta)n, \varepsilon)\big)\right)$$

where χ is the Euler-Poincaré characteristic. One can find an illustration of the index function in [31], Section 3.3. The normal bundle of $X \in \mathcal{U}_{PR}$ is then

$$\mathcal{N}_X = \big\{(x,n) \in \mathbb{R}^d \times S^{d-1} : i_X(x,n) \neq 0\big\} \tag{8}$$

It can be shown ([29]) that $\mathcal{N}_X$ is a $(d-1)$-rectifiable set and the index function can be seen as a multiplicity function for the tangent space of the normal bundle at point x, with direction n. We define the normal cycle for a set $X \in \mathcal{U}_{PR}$ as

$$N(X)(\omega) := \int_{\mathcal{N}_X} \langle i_X(x,n)\omega(x,n) | \tau_{\mathcal{N}_X}(x,n) \rangle \, d\mathcal{H}^{d-1}(x,n) \tag{9}$$

$i_X(x,n)$ can be seen as the multiplicity of the tangent plane of the normal bundle at point (x,n), and is so that this definition of normal cycle is coherent with the additive property (7)

1.2.5. Transport of Normal Cycles with Diffeomorphisms. Now, we have a coherent framework to represent both continuous and discrete shapes. For a matching purpose, we will consider diffeomorphisms transforming our shapes. To fit the shape representation with normal cycles into a matching problem, it is necessary to describe how a diffeomorphism acts on the normal cycle associated with a shape. For this, we define two actions: the *pull-back* action of diffeomorphisms on differential forms, and the dual *push-forward* action on currents:

DEFINITION 21. *Let $\omega \in \Omega_0^m(\mathbb{R}^d)$, $x \in \mathbb{R}^d$ and $\tau_1 \wedge \cdots \wedge \tau_m \in \Lambda^m(\mathbb{R}^d)$, φ a diffeomorphism of $\mathbb{R}^d$.*

- *The* pull-back *action of φ on ω, $\varphi^\sharp\omega$ is:*

$$\big\langle \varphi^\sharp\omega(x) \big| \tau_1 \wedge \cdots \wedge \tau_m \big\rangle = \langle \omega(\varphi(x)) | d\varphi_x.\tau_1 \wedge \cdots \wedge d\varphi_x.\tau_m \rangle$$

- *The* push-forward *action of φ on $T \in \Omega_0^m(\mathbb{R}^d)'$, $\varphi_\sharp T$ is:*

$$\varphi_\sharp T(\omega) = T(\varphi^\sharp\omega)$$

The push-forward action on currents is geometric in the sense that if X is a m-rectifiable set of $\mathbb{R}^d$, then $\varphi^\sharp[X] = [\varphi(X)]$. Since a normal cycle is a current whose support lives in $\mathbb{R}^d \times S^{d-1}$, we will use straightforwardly this action. The question is: given a diffeomorphism φ and a set X with positive reach, in $\mathbb{R}^d$, what is the action of φ on the normal bundle ? Let $(x, n) \in \mathcal{N}_X$. One can show that $\varphi : X \to \varphi(X)$ induces a diffeomorphism $\psi : \mathcal{N}_X \to \mathcal{N}_{\varphi(X)}$:

$$\psi(x, n) = \left(\varphi(x), \frac{d\varphi_x^{-t} n}{\left\|d\varphi_x^{-t} n\right\|}\right)$$

where $d\varphi_x^{-t} = \left(d\varphi_x^{-1}\right)^t$. This diffeomorphism ψ is defined such that the action of a diffeomorphism φ on normal cycles satisfies:

$$\varphi.N(X) = \psi_\sharp N(X) = \psi_\sharp[\mathcal{N}_X] = [\psi(\mathcal{N}_X)] = [\mathcal{N}_{\varphi(X)}] = N(\varphi(X))$$

which is a geometric action as well.

It is possible to explicit this action: one needs to compute $d\psi_{(x,n)}$. As we will see, the second differential of φ is involved, which again is not surprising in view of the link between normal cycles and curvatures. We will compute the differential with respect to x: $d_x\psi_{(x,n)}$ and the differential with respect to n: $d_n\psi_{(x,n)}$. For this, recall that

$$d\left(u \mapsto \frac{u}{\|u\|}\right)_u h = \frac{1}{\|u\|}\left(h - \left\langle h, \frac{u}{\|u\|}\right\rangle \frac{u}{\|u\|}\right)$$

Then, using the chain rule for differentials, and denoting $n' = \frac{d\varphi_x^{-t} n}{\left\|d\varphi_x^{-t} n\right\|}$ we get:

$$d_n\psi_{(x,n)} = \left(0,\ \frac{1}{\left\|d\varphi_x^{-t} n\right\|}\left(d\varphi_x^{-t} - \left\langle n', d\varphi_x^{-t}\right\rangle n'\right)\right)$$

and

$$d_x\psi_{(x,n)} = \left(d\varphi_x,\ -d\varphi_x^{-t} d^2\varphi_x(.,.)^t n' + \left\langle n', d\varphi_x^{-t} d^2\varphi_x(.,.)^t n'\right\rangle n'\right)$$

where $d^2\varphi_x$ is the second differential of φ. If we let $p_{(n')^\perp}$ be the orthogonal projection on $(n')^\perp$, we can write these differentials:

$$\begin{aligned} d_x\psi_{(x,n)} &= \left(d\varphi_x,\ -p_{(n')^\perp} d\varphi_x^{-t} d^2\varphi_x(.,.)^t n'\right) \\ d_n\psi_{(x,n)} &= \left(0,\ p_{(n')^\perp} \frac{d\varphi_x^{-t}}{\left\|d\varphi_x^{-t} n\right\|}\right) \end{aligned} \tag{10}$$

To clarify the notation, let $(x, n) \in \mathbb{R}^d \times S^{d-1}$ and $(\tau, \nu) \in \mathbb{R}^d \times \mathbb{R}^d$. We have

$$d\psi_{(x,n)}.\begin{pmatrix}\tau \\ \nu\end{pmatrix} = \begin{pmatrix} d\varphi_x.\tau \\ \\ -p_{(n')^\perp} d\varphi_x^{-t} d^2\varphi(\tau, .)^t.n' + p_{(n')^\perp} \frac{d\varphi_x^{-t}.\nu}{\left\|d\varphi_x^{-t} n\right\|} \end{pmatrix}$$

To conclude this section, we have seen that the theory of normal cycles is a way to represent shapes as currents with support in $\mathbb{R}^d \times S^{d-1}$. The additive property allows in particular to include polygonal meshes in the setting, and thus to consider both continuous shapes and their discrete representations in the same framework. This representation is independent of the initial orientation of the shapes, and encodes curvature information. Moreover, it can fit well in a matching problem with an explicit action of diffeomorphisms on normal cycles. The next step is now to define a metric on normal cycles in order to have a notion of closeness between shapes.

2. Kernel metrics on normal cycles. The idea of normal cycles (resp. currents) is convenient to embed shapes in a vector space: the space of $(d-1)$-currents in $\mathbb{R}^d \times S^{d-1}$ (resp. the space of m-current in $\mathbb{R}^d$). These spaces, defined as dual of spaces of differential forms, come with a dual norm: if $T \in \Omega_0^m(\mathbb{R}^d)'$, we define $M(T) := \sup\left\{T(\omega), \omega \in \Omega_0^m(\mathbb{R}^d), \|\omega\|_\infty \leq 1\right\}$, called the mass norm in geometric measure theory. It would be tempting to use this norm as a distance between shapes. However this norm is not interesting for a matching purpose. Indeed, if C and S are two m-rectifiable sets, non intersecting, then one can show that $M([S]-[C]) = \mathcal{H}^m(C) + \mathcal{H}^m(S)$, and this independently of any relative closeness between the two sets. This happens because the set of test functions ω is too large, and thus discriminates completely the two shapes. Another norm which turns out to be useful in geometric measure theory is the flat norm:

$$F(T) := \sup\left\{T(\omega), \omega \in \Omega_{1,0}^m(\mathbb{R}^d)\, \|\omega\|_\infty \leq 1,\ \|d\omega\|_\infty \leq 1\right\}$$

where $d\omega$ is the exterior derivative of ω. Though, this distance has several drawbacks, the main one being its non closed form. For our numerical purpose, we need a computable expression for the dissimilarity between shapes. In the very same spirit of [21], we will use kernel metrics on normal cycles as dissimilarity measures. The theory of reproducing kernels comes from the seminal work of [2] and is now widely used in computational anatomy ([21, 15, 11]). A brief reminder of reproducing kernel will be developed in the next section.

2.1. Vector-valued Reproducing Kernel Hilbert Spaces. For a study of some properties of Reproducing Kernel Hilbert spaces in the vectorial case, one can refer to [25].

Let H be a Hilbert space of functions from $\mathbb{R}^d$ to a euclidean space E: $H \subset \mathcal{F}(\mathbb{R}^d, E)$. We denote $\langle .,. \rangle_H$ the scalar product on H and $\langle .,. \rangle_E$ the one on E.

Definition 22 (Reproducing Kernel Hilbert Space). *H is a Reproducing Kernel Hilbert Space if the evaluation functionals $u \in H \mapsto \langle u(x), \alpha \rangle_E$, $\alpha \in E$, $x \in \mathbb{R}^d, u \in H$ are continuous, i.e. $\delta_x^\alpha \in H'$.*

As detailed in [25], a RKHS is canonically associated to a positive definite kernel, and conversely (see again [25] for a definition of positive definite kernel).

For our need, we will rather consider the second aspect: the space H is constructed with a kernel K (e.g. $K(x,y) = \exp\left(-\frac{\|x-y\|}{\sigma^2}\right) \mathrm{Id}$), i.e the kernel K generates a prehilbertian space: $H_0 = \mathrm{Vect}\left\{K(x,.)\alpha | x \in \mathbb{R}^d, \alpha \in E\right\} \subset \mathcal{F}(\mathbb{R}^d, E)$, with scalar product:

$$\left\langle \sum_{i=1}^n K(x_i,.)\alpha_i, \sum_{j=1}^m K(y_j,.)\beta_j \right\rangle := \sum_{i=1}^n \sum_{j=1}^m \langle \alpha_i, K(x_i,y_j)\beta_j \rangle_E$$

so that the scalar product, and the norm is explicit. The space H is obtained by completion of H_0 with respect to the scalar product (see [2] for technical details). This theory is widely used in computational anatomy either to have an explicit distance between shapes (as we will see in the next paragraph) or to have a space of deformations whose equations are easy to implement numerically.

2.2. Kernel metrics on currents. The theory of reproducing kernel provides a powerful tool to construct a Hilbert space with explicit scalar product. We will see how to use it in the context of currents. All this has been developed in [21], [32].

In [21], J. Glaunès defines a RKHS W in the space of m-differential forms $\Omega_0^m(\mathbb{R}^d)$ (i.e. with the previous notation, $E = \Lambda^m(\mathbb{R}^d)^*$) using a positive definite kernel K_W. We suppose that $W \hookrightarrow \Omega_0^m(\mathbb{R}^d)$, i.e. for every $\omega \in W$, $\|\omega\|_\infty \leq c\,\|\omega\|_W$. Then if S is a compact, m-rectifiable set of $\mathbb{R}^d$, we have

$$|S(\omega)| \leq \int_S |\omega| \leq \mathcal{H}^m(S) c\,\|\omega\|_W \tag{11}$$

so that the restriction of $[S]$ to W belongs to W'. Hence a m-rectifiable set can be considered as an element of the Hilbert W', whose norm is explicit by the reproducing kernel. This raises the question of choosing a positive definite kernel on the space of differential forms. Here we will use scalar kernels: we define for every $\alpha, \beta \in \Lambda^m(\mathbb{R}^d)$, for every $x, y \in \mathbb{R}^d$

$$\langle K_W(x,y)\alpha, \beta\rangle_{\Lambda^m(\mathbb{R}^d)} = k_W(x,y)\,\langle \alpha, \beta\rangle_{\Lambda^m(\mathbb{R}^d)}$$

where k_W is a scalar kernel, for example $k_W(x,y) = \exp\left(\frac{-|x-y|^2}{\sigma_W^2}\right)$, with σ_W a parameter. This is a positive definite kernel (see [2] for example) and defines a RKHS W of m-differential forms. We have to be sure that this kernel defines a RKHS W embedded in the space $\Omega_0^m(\mathbb{R}^d)$:

Proposition 23 ([21], Chap 2. Th. 9). *Let $p \in \mathbb{N}$, and a positive definite kernel $K : \mathbb{R}^d \times \mathbb{R}^d \to \mathcal{L}(E)$, with derivatives at order $\leq 2p$ which are continuous and bounded. Suppose that for every $x \in \mathbb{R}^d$, $K(x,.)$ vanishes at infinity, and so do its derivatives at order $\leq p$. Then the RKHS W associated with K is embedded into $\mathcal{C}_0^p(\mathbb{R}^d, E)$.*

All the kernels in this paper will fulfill the previous proposition. For example a scalar Gaussian kernel guarantees that its RKHS is embedded in a space as regular as we want ($\forall p \in \mathbb{N}, W \hookrightarrow \mathcal{C}_0^p(\mathbb{R}^d, E)$).

Now let S be a m-rectifiable set in $\mathbb{R}^d$, $\alpha \in \Lambda^m(\mathbb{R}^d)$, and $x \in \mathbb{R}^d$. From the reproducing property, we have

$$\begin{aligned}\langle \alpha, \mathcal{K}_W[S](x)\rangle_{\Lambda^m(\mathbb{R}^d)} &= \langle \delta_x^\alpha | \mathcal{K}_W[S]\rangle \\ &= \langle [S] | K_W(x,.)(\alpha,.)\rangle \\ &= \int_S k_W(x,y)\,\langle \alpha, \tau_S(y)\rangle\, d\mathcal{H}^m(y).\end{aligned}$$

Thus the scalar product between two m-rectifiable orientable sets S and C can be expressed as

$$\langle [S], [C]\rangle_{W'} = \int_S \int_C k_W(x,y)\,\langle \tau_S(x), \tau_S(y)\rangle_{\Lambda^m(R^d)}\, d\mathcal{H}^m(x) d\mathcal{H}^m(y) \tag{12}$$

where $\tau_S(x)$ is the m-vector associated with a positively oriented orthonormal basis of $T_x S$.

The distance between two shapes S and C is then

$$d(C,S)^2 = \|[S] - [C]\|_{W'}^2 = \langle [S], [S]\rangle_{W'} - 2\,\langle [S], [C]\rangle_{W'} + \langle [C], [C]\rangle_{W'}$$

2.3. Kernel metrics on normal cycles. Normal cycles are $(d-1)$-currents on the space $\mathbb{R}^d \times S^{d-1}$, $\Omega_0^{d-1}(\mathbb{R}^d \times S^{d-1})'$. Thus, the previous construction can be used to define a distance between shapes as the norm of the difference of their normal cycles for a given kernel metric. This requires only to choose a scalar positive definite kernel k on $\mathbb{R}^d \times S^{d-1}$. We define k as a product of two positive definite kernel: a point kernel k_p and a normal kernel k_n:

$$k((x,u),(y,v)) = k_p(x,y)k_n(u,v)$$

which is a positive definite kernel ([2]). Defining k as a product of two kernels is justified by the fact that the point-space $\mathbb{R}^d$ and the normal-space S^{d-1} have different geometric meanings and therefore should be considered separately. We can choose $k_p(x,y) = \exp\left(\frac{-|x-y|^2}{\sigma_W^2}\right)$ a Gaussian kernel or $k_p(x,y) = \frac{1}{1+\frac{|x-y|^2}{\sigma_W^2}}$ a Cauchy kernel. For the normal kernel k_n we will chose a reproducing kernel of a Sobolev space $H^s(S^{d-1})$ of order s. Even if the expression of this Sobolev kernel is not explicit at first, we will see that it can be expressed with spherical harmonics when dealing with three dimensional problems. Now the reproducing kernel for normal cycles will be $\langle K_W((x,u),(y,v))\eta,\nu\rangle_{\Lambda^{d-1}(\mathbb{R}^d\times\mathbb{R}^d)} = k_p(x,y)k_n(u,v)\langle\eta,\nu\rangle_{\Lambda^{d-1}(\mathbb{R}^d\times\mathbb{R}^d)}$ with $x,y\in\mathbb{R}^d$, $u,v\in S$, $\eta,\nu\in\Lambda^{d-1}(\mathbb{R}^d\times\mathbb{R}^d)$.

Remark 24. Instead of the canonical scalar product on $\mathbb{R}^d\times\mathbb{R}^d$, we can choose a weighted scalar product, as for example: $\langle(\tau_1,\nu_1),(\tau_2,\nu_2)\rangle_\lambda := \tau_1\cdot\tau_2 + \lambda\nu_1\cdot\nu_2$, where $\tau_i,\nu_i\in\mathbb{R}^d$ and $\lambda>0$. The scalar product on $\Lambda^{d-1}(\mathbb{R}^d\times\mathbb{R}^d)$ is then:

$$\langle u_1\wedge\cdots\wedge u_{d-1}, v_1\wedge\cdots\wedge v_{d-1}\rangle_\lambda := \det\left(\langle u_i,v_i\rangle_\lambda\right)$$

where $u_i,v_i\in\mathbb{R}^d\times\mathbb{R}^d$. This introduces a new weight parameter in the model, but is justified again by the fact that the two $\mathbb{R}^d$ spaces in the cartesian product have different geometric meanings. Also, as we will see in section 5, when analyzing homogeneity properties of the functional with respect to scaling, it seems clear that λ should depend on the scale σ_W of the space kernel k_p.

PROPOSITION 25. *If k_p is a scalar kernel, $k_p(x,.)\in\mathcal{C}_0^1(\mathbb{R}^d,\mathbb{R})$, k_n is the reproducing kernel of $H^s(S^{d-1})$, $s>\frac{d+1}{2}$, then $W\hookrightarrow\mathcal{C}_0^1\left(\mathbb{R}^d\times S^{d-1},\Lambda^{d-1}(\mathbb{R}^d\times\mathbb{R}^d)\right)$.*

Proof. If we choose $s>\frac{d+1}{2}$ for the Sobolev kernel k_n, then we have Sobolev injections (see [7], Chap. IX. The results can be applied straightforwardly to the case of compact submanifolds without boundaries using partition of unity on a finite atlas of the manifold): $H^s(S^{d-1})\hookrightarrow\mathcal{C}^j(S^{d-1})$, $\forall 0\le j<s-\frac{d-1}{2}$. Thus if $s>\frac{d+1}{2}$, $H^s(S^{d-1})\hookrightarrow\mathcal{C}^1(S^{d-1})$. K_W, which is a tensor product of k_p and k_n is such that $\partial_1\partial_2 K$ (with the same notations as [25]) exists, and is continuous, and locally bounded. Moreover, $K_W(.,(x,u))\tau\in\mathcal{C}_0^1\left(\mathbb{R}^d\times S^{d-1},\Lambda^{d-1}\left(\mathbb{R}^d\times\mathbb{R}^d\right)\right)$ because $k_p(x,.)\in\mathcal{C}_0^1(\mathbb{R}^d,\mathbb{R})$. By Theorem 2.11 of [25], we conclude that $W\hookrightarrow\mathcal{C}_0^1\left(\mathbb{R}^d\times S^{d-1},\Lambda^{d-1}(\mathbb{R}^d\times\mathbb{R}^d)\right)$. ∎

And for the same reason as for classical currents (see (11)), for every S set with positive reach, $N(S)\in W'$. Thus the Hilbert norm on W' is a dissimilarity measure for normal cycles. The fact that this norm is a proper metric on the space $\Omega_0^{d-1}(\mathbb{R}^d\times S^{d-1})'$ is not obvious and is postponed to subsection 2.5.

The scalar product between two shapes S and C (which are both sets with positive reach) is

$$\langle N(C), N(S)\rangle_{W'} = \int_{\mathcal{N}_C}\int_{\mathcal{N}_S} k_p(x,y)k_n(u,v)\,\langle \tau_{\mathcal{N}_S}(x,u), \tau_{\mathcal{N}_C}(y,v)\rangle_{\Lambda^{d-1}(\mathbb{R}^d\times\mathbb{R}^d)} \, d\mathcal{H}^{d-1}(x,u)d\mathcal{H}^{d-1}(y,v) \tag{13}$$

The kernel in this formula takes into account both the spatial localization and the normal position through the kernel and the tangent plane of the normal bundle ($\langle \tau_{\mathcal{N}_S}(x,u), \tau_{\mathcal{N}_C}(y,v)\rangle$). The square of the distance between shapes is then:

$$\mathrm{d}(S,C)^2 = \|N(S) - N(C)\|^2_{W'} = \langle N(S), N(S)\rangle_{W'} + \langle N(C), N(C)\rangle_{W'} - 2\langle N(S), N(C)\rangle_{W'} \tag{14}$$

2.4. Reproducing kernel on S^2. As we said before, we consider some Sobolev space $H^s(S^2)$. For $s > 2$, we have $H^s(S^2) \hookrightarrow \mathcal{C}^1(S^2)$, and $H^s(S^2)$ is a reproducing kernel. We denote it k_n. In order to have an explicit expression of k_n, we will use expansion on spherical harmonics (See Appendix A). We recall that the spherical harmonics $(Y_{l,m})$, for $l \in \mathbb{N}, -l \leq m \leq l$ form an Hilbert frame of $L^2(S^2)$. The operator associated with k_n is $L = (\mathrm{Id} - \Delta)^s$. And we have by definition of L: $Lk_n(x,.) = \delta_x$. Using an expansion on spherical harmonics of $k_n(x,.)$ for $x \in S^2$, we get $k_n(x,.) = \sum_{l\in\mathbb{N}}\sum_{m=-l}^{l}\alpha_{l,m}(x)Y_{lm}$. By the reproducing property, we have

$$\langle k_n(x,.), Y_{l',m'}\rangle_{H^s(S^2)} = Y_{l'm'}(x)$$

And also, by definition of the scalar product and the operator L:

$$\begin{aligned}\langle k_n(x,.), Y_{l',m'}\rangle_{H^s(S^2)} &= \langle k_n(x,.), LY_{l'm'}\rangle_{L^2(S^2)} \\ &= \left\langle \sum_{l\in\mathbb{N}}\sum_{m=-l}^{l}\alpha_{l,m}(x)Y_{lm}, (1+l(l+1))^s Y_{l'm'}\right\rangle_{L^2(S^2)} \\ &= \alpha_{l'm'}(x)(1+l(l+1))^s = Y_{l'm'}(x)\end{aligned}$$

which gives:

$$k_n(x,y) = \sum_{l\in\mathbb{N}}\sum_{m=-l}^{l}\frac{1}{(1+l(l+1))^s}Y_{lm}(x)Y_{lm}(y) \tag{15}$$

This is the kernel we will use for computational purpose in the following sections.

Remark 26. Conversely, we could have fixed the eigenvalues λ_l at first instead of $1 + l(l+1)$, and defined the kernel k_n as in (15). All rotation invariant reproducing kernels on the sphere can be obtained with this procedure. Although we only consider kernels associated to Sobolev spaces in this work, one may definitely consider general metrics here by specifying appropriate assumptions on the sequence of eigenvalues.

2.5. Universality. As explained previously, the kernel setting provides a dissimilarity measure between shapes through the expression (14). In this subsection we tackle briefly whether or not this dissimilarity measure is a real distance.

With Proposition 25 we have a continuous injection $j : W \hookrightarrow \Omega_0^{d-1}(\mathbb{R}^d \times S^{d-1})$. However the dual metric that we use on normal cycles comes from the continuous dual application :

$$j^* : \Omega_0^{d-1}(\mathbb{R}^d \times S^{d-1})' \to W'$$

which may not be injective. This results in a pseudo distance only : it may be possible to have $N, M \in \Omega_0^{d-1}(\mathbb{R}^d \times S^{d-1})'$, $N \neq M$ with $\|j^*(N) - j^*(M)\|_{W'} = 0$. Thus, we have no guarantee that the distance (14) is a proper distance. We will prove here that with some specific kernels k_p and k_n, this does not happen, and thus the dissimilarity measure is a proper distance.

Using a corollary of the Hahn-Banach theorem ([7], Corollary 1.8), it can be shown that j^* is injective if, and only if W is dense in $\Omega_0^{d-1}(\mathbb{R}^d \times S^{d-1})$. This density property of a RKHS in a space of continuous functions is called the $\mathcal{C}^0$**-universality** of the kernel. It has first interest in machine learning with kernels as it guarantees that any continuous target function can be approximate using the kernel. It has been studied for scalar kernels in [24], and in the case of vector valued kernels in [8]. Note that the universality is also useful for optimal interpolation in Hilbert subspaces [33], chapter 4. As far as we know, this point of universality has been first addressed in the setting of dissimilarity measure for shapes in [12], with kernel metrics on varifolds.

THEOREM 27. d *defined in* (14) *is a distance on* $\Omega_0^{d-1}(\mathbb{R}^d \times S^{d-1})$.

In our framework, we have a RKHS W, with kernel $K_W : (\mathbb{R}^d \times S^{d-1})^2 \to \mathcal{L}\left(\Lambda^{d-1}(\mathbb{R}^d \times \mathbb{R}^d)\right)$, with $K_W((x,u),(y,v)) = k_p(x,y)k_n(u,v)\mathrm{Id}_{\Lambda^{d-1}(\mathbb{R}^d \times \mathbb{R}^d)}$. Using Example 14 in [8], K_W is a universal kernel if, and only if $k_p \otimes k_n$ is a universal scalar kernel. Moreover, using Example 15 of the same reference, for $k_p \otimes k_n$ to be universal, it is sufficient that k_p and k_n are universal. We are left to show that both k_p and k_n are universal. In our applications, k_p will be a Gaussian kernel, which is universal (see [8] or [24]). For the normal kernel k_n, we will make use of the expansion in spherical harmonics : indeed, we recall that we choose $k_n(x,y) = \sum_{l \in \mathbb{N}} \sum_{m=-l}^{l} \frac{1}{(1+l(l+1))^s} Y_{lm}(x) Y_{lm}(y)$. Using theorem 7 of [24], and the fact that the spherical harmonics are dense in $\mathcal{C}(S^2)$ for the norm of uniform convergence ([20], Prop. 1.6), we get that k_n is a universal kernel as well. Thus the reproducing kernel K_W is a $\mathcal{C}^0$-universal kernel and the dual application j^* is one-to-one, which proves that d defined in (14) is a proper distance on normal cycles.

3. Computational framework. The aim of this section is to derive all the theory developed in this article into the special case of a polyhedral approximation of shapes. Expression (13) is the key to compute distance between shapes, and it can be simplified a lot when dealing with discrete approximations as we will see later on. We will compute (13) in the case of a union of segments in $\mathbb{R}^3$.

3.1. Convergence towards the continuous shape. In the former sections we have seen the reproducing kernel theory, applied to obtain an explicit metric on the space of $(d-1)$-currents on $\mathbb{R}^d \times S^{d-1}$ (and in particular on the normal cycles associated with union of sets with positive reach). Now in computational anatomy, a continuous shape is approximated with a polyhedral shape. In order to have a consistent framework, we would like that the normal cycle of the approximation we are dealing with is not too far from the theoretical one. Or at least having a convergence result for the kernel metric when the diameter of meshes is close to 0. The theorem we will use here is from J. Fu [18]. In order to have a convergence result for normal cycle, we have to keep in mind some pathological examples as the Schwarz polyhedron (see the discussion in [28]): it is possible to have a polyhedral approximation of a cylinder,

with diameter of meshes going to zero, and yet the area of the approximations blowing up. And as a consequence of Theorem 18 and discussion below, the convergence of normal cycles implies the convergence of areas. This is why it seems necessary to have a control of the way diameters tend towards 0. More precisely for the next result, we will need the notion of *fatness* of a triangulation.

DEFINITION 28. *Let T be a k-simplex, with vertices $v_0, \dots, v_k$. The* size *of T is*

$$\eta(T) := \max |v_i - v_j|$$

The fatness *of T is*

$$\Theta(T) := \min \left\{ \frac{\mathcal{H}^j(\mu)}{\eta(T)^j}, \mu \text{ is a } j \text{ dimensional face of } T, j = 0, \dots, k \right\}$$

Let Δ be a triangulation. The fatness *of Δ is*

$$\Theta(\Delta) := \min \{\Theta(T), T \text{ is a } k\text{-simplex of } \Delta\}$$

This definition of fatness is less restrictive than the usual definition because it takes into account all the j-dimensional faces. Bounding below the fatness of a triangulation guarantees that the angles of the triangles are not too close to 0. Hence we avoid pathological cases as the Schwarz polyhedron.

Now let X be a smooth submanifold in $\mathbb{R}^d$. To have a convergence result for the approximations, we will demand that the approximations are *closely inscribed* in X:

DEFINITION 29. *A triangulation Δ is* inscribed *in X if:*
1. *All vertices of Δ lie in X*
2. *All vertices of $\partial\Delta$ lie in ∂X.*

Δ is closely inscribed *in X if, additionally:*
1. *$\Delta \subset X_r$ and the projection on X restricted to Δ is one-to-one.*
2. *$\partial\Delta \subset (\partial X)_r$ and the projection on ∂X restricted to $\partial\Delta$ is one-to-one.*

We can now state J. Fu's theorem:

THEOREM 30. *Let $(P^n)_{n\in\mathbb{N}}$ be a sequence of triangulations of a smooth submanifold X in $\mathbb{R}^d$, closely inscribed in X. Suppose that $P^n \to X$ and $\partial P^n \to \partial X$ in the Hausdorff metric on subsets of $\mathbb{R}^d$, and that for every $n \in \mathbb{N}$, $\Theta(P^n) \geq c$, for some constant $c > 0$. Then $N(P^n) \xrightarrow[n\to\infty]{} N(X)$ for the flat metric.*

The proof of this theorem is far beyond the scope of this article, thus we will only make a few remarks on it. The proof relies on the theory of compactness for integral currents (see [17], 4.2) coupled with a uniqueness result for normal cycles ([19], 3.). A direct corollary is the convergence of the curvatures of the approximations, in the sense of weak convergence for measures. It can be obtained using the Lipschitz-Killing differential forms (Definition 17, [36], [27] chap. 21). Since this theorem uses compactness, it prevents us from a quantification of the rate of convergence. Note that in [14], [27], the authors use a different argument in order to have a bound for the convergence of curvature measures and tensors, using normal cycles.

This theorem guarantees that under not so restrictive conditions on the triangulations, we have convergence of the normal cycles of the approximations towards the normal cycle of the smooth manifold, for the flat norm. Then it is sufficient that W is continuously embedded in $\Omega^{d-1}_{1,0}(\mathbb{R}^d \times S^{d-1})$ equipped with the flat norm to have the same result with the kernel metric. The next proposition shows that it depends only on the regularity of the kernel.

PROPOSITION 31. *Let k be a positive kernel on the product space $\mathbb{R}^d \times S^{d-1}$, such that k is twice continuously differentiable, with bounded first derivatives. Suppose in addition that for any $(x,u) \in \mathbb{R}^d \times S^{d-1}$, $k((x,u),.)$ and its first order derivative vanish at infinity. Then, the RKHS associated with k is continuously embedded in $\Omega_{1,0}^{d-1}(\mathbb{R}^d \times S^{d-1})$ with the flat norm on differential forms.*

Proof. Following the proof of [21], theorem 9, chapter 2, we can show that for any $\omega \in W$,

$$\|\omega\|_{1,\infty} \leq \sqrt{\|k\|_{2,\infty}}\, \|\omega\|_W .$$

Here $\|\omega\|_{1,\infty} = \|\omega\|_\infty + \|D\omega\|_\infty$, where $D\omega$ refers to the differential of ω, *i.e.* ω is seen as an application from $\mathbb{R}^d \times S^{d-1}$ to the vector space $\Lambda^{d-1}(\mathbb{R}^d \times \mathbb{R}^d)^*$. This is not exactly the flat norm, which is $\|\omega\|_F := \|\omega\|_\infty + \|d\omega\|_\infty$, where $d\omega$ designates the exterior derivative of ω. However $\|\omega\|_F \leq cste\, \|\omega\|_{1,\infty}$. $d\omega(x,u)$ is indeed obtained by making $D\omega(x,u)$ into an alternating map in all of its d arguments (and not only in the last $d-1$ ones):

$$d\omega(x,u)(v_1 \wedge \cdots \wedge v_d) = \sum_{i=1}^{d} (-1)^i D\omega(x,u)(v_i)(v_1 \wedge \cdots \wedge v_{i-1} \wedge v_{i+1} \wedge \cdots \wedge v_d)$$

where $v_i \in \mathbb{R}^d$. Thus a control of the uniform norm of $D\omega$ ensures a control on the uniform norm of $d\omega$. So, there exists $C > 0$ such that for every $\omega \in \Omega_0^{d-1}(\mathbb{R}^d \times S^{d-1})$

$$\|\omega\|_F \leq C\sqrt{\|k\|_{2,\infty}}\, \|\omega\|_W$$

∎

which proves the embedding.

Thereby, the dual application $j^* : \Omega_{1,0}^{d-1}(\mathbb{R}^d \times S^{d-1})' \hookrightarrow W'$ is continuous and injective with Theorem 27, and provides a distance on $\Omega_{1,0}^{d-1}(\mathbb{R}^d \times S^{d-1})'$, resulting for the Hilbert structure of the RKHS W. This, combined with theorem 30 guarantees the convergence of the approximations for the kernel metric on normal cycles, under the same conditions.

THEOREM 32. *Let $(P^n)_{n\in\mathbb{N}}$ be a sequence of triangulations of a smooth submanifold X in $\mathbb{R}^d$, closely inscribed in X. Suppose that $P^n \to X$ and $\partial P^n \to \partial X$ in the Hausdorff metric on subsets of $\mathbb{R}^d$, and that for every $n \in N$, $\Theta(P^n) \geq c$, for some constant $c > 0$. Then $N(P^n) \underset{n\infty}{\longrightarrow} N(X)$ for the kernel metric.*

Remark 33. The assumption of closely inscribed triangulations is quite restrictive compared to some assumptions that one can find in the Γ-convergence for functional shapes with varifold norm ([10]), or in curvature approximation of smooth surfaces ([14]). We did not investigate much yet to relax it, however it does not seem immediate since we use Theorem 30, whose proof relies on this hypothesis.

3.2. Representation of Discrete Curves with Normal Cycles.

3.2.1. Decomposition of the Normal Cycle for Unions of Segments. The intersection of two non parallel segments is either empty or a single point. This means that we can always consider the normal cycle associated with an intersection of two segments. Thus, the formula (7) makes always sense when dealing with a union of segments. However, this formula is not ready to use. In order to overcome this difficulty, we introduce here a new decomposition of the normal bundle of a union

of segments. As we will see, this decomposition will make the additive property straightforward and the normal cycle of each part of this cutting will be explicit.

Let $a, b \in \mathbb{R}^d$ and $C = [a, b]$ be the segment with extremities a and b. We denote $\tilde{C} = C \setminus \{a, b\}$. Following the reasoning in Example 11 one can make explicit the normal bundle of C. The notations are the same as in Definition 8: for $x \in \tilde{C}$, $\mathrm{Nor}(C, x)$ is a $(d-2)$-sphere, orthogonal to C: $\mathrm{Nor}(C, x) = (b-a)^\perp \cap S^{d-2}$. For $x = a$ or b, $\mathrm{Nor}(C, x)$ is a half $(d-1)$-sphere, oriented in the outward direction to the segment: $\mathrm{Nor}(C, a) = S^+_{a-b}$ and $\mathrm{Nor}(C, b) = S^+_{b-a}$, where we recall that $S^+_u = \{v \in S^{d-1} | u.v \geq 0\}$.

Thus, the unit normal bundle is composed of two parts, a cylindrical part and a spherical part. By cylindrical part, we mean a subset of the normal bundle whose tangent spaces have one dimension in the spatial space and one dimension in the normal space. By a spherical part, we mean a subset for which the tangent spaces all belong to the normal space. More precisely, $\mathcal{N}_C = \mathcal{N}_C^{cyl} \cup \mathcal{N}_C^{sph}$ with $\mathcal{N}_C^{cyl} := \tilde{C} \times ((b-a)^\perp \cap S^{d-1})$ and $\mathcal{N}_C^{sph} := (\{a\} \times S^+_{a-b}) \cup (\{b\} \times S^+_{b-a})$. These two parts are disjoint and the normal cycle $N(C)$ satisfies $N(C) = N(C)^{cyl} + N(C)^{sph}$ with $N(C)^{cyl} := [\mathcal{N}_C^{cyl}]$ and $N(C)^{sph} := [\mathcal{N}_C^{sph}]$.

In order to get a nice decomposition in the case of unions of segments, it is convenient to define the normal cycle associated to the "open" segment $\tilde{C}$ as: $N(\tilde{C}) := N(C) - N(\{a\}) - N(\{b\})$. Since the normal bundles of $\{a\}$ and $\{b\}$ are entire spheres, we see that $N(\tilde{C})$ expresses also as a sum of a cylindrical part and a spherical part: $N(\tilde{C}) = N(C)^{cyl} + N(\tilde{C})^{sph}$ with $N(\tilde{C})^{sph} := -[\{a\} \times S^+_{b-a}] - [\{b\} \times S^+_{a-b}]$.

Now let $C_1 \cup \cdots \cup C_n$ be a union of n segments in $\mathbb{R}^d$. We can consider without loss of generality that the intersection of two segments $C_i \cap C_j$ is either empty or composed of a single point. Using the additive property (7) and the previous definition of the normal cycles of an "open" segment, it can be easily seen that the normal cycle of a union of segments can be obtained by summing the normal cycles associated to open segments and vertices. More precisely, if we denote $\{v_1, \ldots, v_N\}$ the vertices of $\cup_{i=1}^n C_i$, our decomposition of the normal bundle satisfies:

$$N(C_1 \cup \cdots \cup C_n) = \sum_{i=1}^{n} N(\tilde{C}_i) + \sum_{j=1}^{N} N(\{v_i\}) \tag{16}$$

Even though the additive property is now straightforward, we will go a bit further in this decomposition, as it will prove to be more efficient with the kernel metric. We can decompose (16) into cylindrical and spherical parts as follows:

$$N(C_1 \cup \cdots \cup C_n) = \left(\sum_{i=1}^{n} N(C_i)^{cyl} \right) + \left(\sum_{i=1}^{n} N(\tilde{C}_i)^{sph} + \sum_{j=1}^{N} N(\{v_i\}) \right) \tag{17}$$

This decomposition is sketched in Figure 2.

Remark 34. A slightly more complex decomposition would be necessary for a union of triangles in $\mathbb{R}^3$, and would involve also a planar part (two dimensions in the spatial space, zero in the normal space). We do not investigate this in this work. Note that the description of the normal cycle of a 2-dimensional polyhedral has been studied in [14]

3.2.2. Approximation of the Normal Cycle for Unions of Segments. In order to get a simple formula for the kernel metric for unions of segments, we now

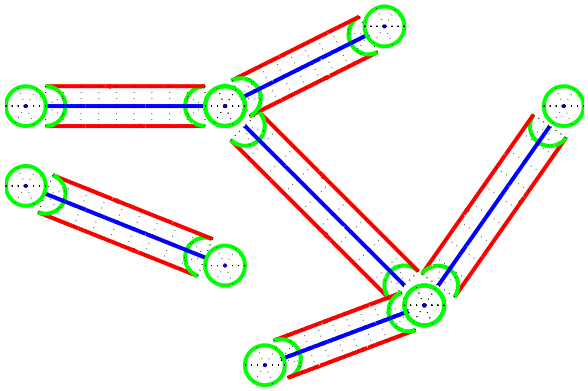

FIG. 2. *Decomposition of the normal bundle of a union of segments. In green, the spherical part (of a single point and of an extremity) and in red the cylindrical part. Note that this representation is only illustrative, as the true normal bundle belongs to the space* $\mathbb{R}^2 \times S^1$ *in this case.*

approximate the cylindrical part of the normal cycle using Dirac evaluation functionals in the space of currents. We denote $x_1, \dots, x_{N_C}$ (resp. $y_1, \dots, y_{N_S}$) the vertices of C (resp. of S) and $f_i = x_{f_i^2} - x_{f_i^1}, 1 \leq i \leq n_C$ (resp. $g_j = y_{g_j^2} - y_{g_j^1}, 1 \leq j \leq n_S$) the edges of C (resp. S). For an edge f_i, $x_{f_i^1}$ and $x_{f_i^2}$ are its two vertices. Moreover, we define $c_i = \frac{1}{2}(x_{f_i^1} + x_{f_i^2})$, $d_j = \frac{1}{2}(y_{g_j^1} + y_{g_j^2})$ the middles of the edges f_i and g_j, and, $\theta_{ij} = \arccos\left(\left\langle \frac{f_i}{|f_i|}, \frac{g_j}{|g_j|} \right\rangle\right)$ the unoriented angle between f_i and g_j ($\theta_{ij} \in [0, \pi]$). We will now define the following approximation of the normal cycles $N(C)$ and $N(S)$:

DEFINITION 35. *For any* $x, v \in \mathbb{R}^d$, $v \neq 0$, *we define* $\delta_{x,v^\perp}$ *as the current such that for any* $(d-1)$*-form* ω *in* $\mathbb{R}^d \times S^{d-1}$,

$$\delta_{x,v^\perp}(\omega) = \int_{S_v^\perp} \langle \omega(x,n) | (v,0) \wedge \nu(n) \rangle \, d\mathcal{H}^{d-2}(n),$$

with $S_v^\perp := S^{d-1} \cap v^\perp$ *and* $\nu(n) = (0, u_1) \wedge \ldots \wedge (0, u_{d-2})$ *such that* $(v/\|v\|, u_1, \dots, u_{d-2}, n)$ *is a positively oriented orthonormal basis. Next we define*

$$N(C)_{approx} := N(C)^{sph} + N(C)^{cyl}_{approx},$$

with

$$N(C)^{cyl}_{approx} := \sum_{i=1}^{n_C} \delta_{c_i, f_i^\perp}.$$

Similarly, $N(S)_{approx} := N(S)^{sph} + N(S)^{cyl}_{approx}$ *with*

$$N(S)^{cyl}_{approx} := \sum_{j=1}^{n_S} \delta_{d_j, g_j^\perp}.$$

In short, this means we approximate integration of the differential form in the spatial domain by a single evaluation, and keep integration in the normal domain. This choice can be intuitively justified by the following reasoning: when considering a sequence of polygonal approximations of possibly non regular curves, the length of segments will always tend towards zero but some angles between segments will remain large.

3.2.3. Computation of the Kernel Metric for Unions of Segments. In this section, we will apply the decomposition of the normal cycle (17) with the framework of kernel metric on normal cycles in order to get an explicit expression of the distance between two discretized curves. We use the kernel metric presented in subsection 2.3.

Let $C = C_1 \cup \cdots \cup C_{n_C}$, $S = S_1 \cup \cdots \cup S_{n_S}$ be two unions of segments in $\mathbb{R}^d$. The calculation of the expression of (13) in this case is simplified by the following property:

PROPOSITION 36. *For any two unions of segments C and S, the cylindrical part $N(C)^{cyl}$ and the approximated cylindrical part $N(C)^{cyl}_{approx}$ are orthogonal to the spherical part $N(S)^{sph}$ with respect to the kernel metric presented in subsection 2.3:*

$$\left\langle N(C)^{cyl}, N(S)^{sph} \right\rangle_{W'} = \left\langle N(C)^{cyl}_{approx}, N(S)^{sph} \right\rangle_{W'} = 0.$$

Proof. Equation (13) takes into account the scalar product in $\Lambda^{d-1}(\mathbb{R}^d \times \mathbb{R}^d)$ between the tangent spaces of the two normal bundles we are considering. Here, we are interested in the scalar product between a cylindrical part, or approximated cylindrical part, and a spherical part. The respective typical $d-1$-vector associated with the tangent spaces are of the form $\tau = (\tau_1, 0) \wedge (0, \tau_2) \wedge \ldots \wedge (0, \tau_{d-1})$ and $\nu = (0, \nu_1) \wedge \ldots \wedge (0, \nu_{d-1})$, and the scalar product between those two vectors is:

$$\langle \tau, \nu \rangle = \begin{vmatrix} (\tau_1,0).(0,\nu_1) & (\tau_1,0).(0,\nu_2) & \cdots & (\tau_1,0).(0,\nu_{d-1}) \\ (0,\tau_2).(0,\nu_1) & (0,\tau_2).(0,\nu_2) & \cdots & (0,\tau_2).(0,\nu_{d-1}) \\ \vdots & \vdots & & \vdots \\ (0,\tau_{d-1}).(0,\nu_1) & (0,\tau_{d-1}).(0,\nu_2) & \cdots & (0,\tau_{d-1}).(0,\nu_{d-1}) \end{vmatrix} = 0$$

since all coefficients in the first line of the above matrix equal to zero. Thus the scalar product of a cylindrical part and a spherical part of normal cycles vanishes. ∎

Remark 37. If we consider the weighted scalar product on $\mathbb{R}^d \times \mathbb{R}^d$ (see Note 24), then it can be easily shown that we have:

$$\langle N(C), N(S) \rangle_{W'_\lambda} = \left\langle N(C)^{cyl}, N(S)^{cyl} \right\rangle_{W'} + \lambda \left\langle N(C)^{sph}, N(S)^{sph} \right\rangle_{W'}$$

where $\langle \cdot, \cdot \rangle_{W'_\lambda}$ denotes the Hilbert metric induced by the weighted metric on $\mathbb{R}^d \times \mathbb{R}^d$.

We see here how convenient the decomposition (17) is: we only need to compute scalar products between spherical parts, and scalar products between cylindrical parts. That is what we will do right below.

We sum up the context: we choose the kernel metric on normal cycles to be as in subsection 2.3, with normal kernel k_n as in subsection 2.4. The computation of the scalar product between $N(C)_{approx}$ and $N(S)_{approx}$ for the kernel metric uses expansions in spherical harmonics for the normal part. This leads to :

THEOREM 38. *One has*

$$\langle N(C)_{approx}, N(S)_{approx}\rangle_{W'} = \left\langle N(C)^{cyl}_{approx}, N(S)^{cyl}_{approx}\right\rangle_{W'} + \left\langle N(C)^{sph}, N(S)^{sph}\right\rangle_{W'}$$

with

$$\left\langle N(C)^{cyl}_{approx}, N(S)^{cyl}_{approx}\right\rangle_{W'} = \sum_{i=1}^{n_C}\sum_{j=1}^{n_S} k_p(c_i, d_j)\,\langle f_i, g_j\rangle \sum_{m\geq 0} a_m \cos(m\theta_{ij}) \tag{18}$$

and

(19)

$$\begin{aligned}\left\langle N(C)^{sph}, N(S)^{sph}\right\rangle_{W'} = &\sum_{k=1}^{N_C}\sum_{l=1}^{N_S} k_p(x_k, y_l)\left(1 - \frac{n_{x_k} + n_{y_l}}{2}\right)\beta \\ &+ \sum_{i=1}^{n_C}\sum_{j=1}^{n_S}\sum_{a,b=1}^{2}\left(b_0 + (-1)^{a+b}\sum_{m\geq 0} b_m \cos(m\theta_{ij})\right) k_p(x_{f_i^a}, y_{g_j^b})\end{aligned}$$

where n_{x_k} (resp. n_{y_l}) is the number of edges adjacent to the vertex x_k (resp. y_l).

Proof. The first equality comes directly from the orthogonality condition of 36. The two formulas are derived in Appendix C and Appendix D. ∎

The constant β and the a_m and b_m coefficients have explicit expansions in spherical harmonics, and are pre-computable. See Appendix C and Appendix D, for their expressions. Here, we just precise that the $(a_m)_{m\geq 0}$ and $(b_m)_{m\geq 0}$ vanish for m even. This is compatible with the fact that normal cycles are unoriented objects: by inverting the orientation of the edges (i.e. if we invert $x_{f_i^1}$ and $x_{f_i^2}$), the scalar product remains unchanged. With these two scalar products, we have all we need to implement an algorithm which computes dissimilarity between two discrete curves. This is the first step to have a matching algorithm.

Computational complexity. The computational complexity of the normal cycle metric, assuming we truncate the spherical harmonics expansions at a fixed order, is of order $O(n_C^2 + N_C^2)$, with n_C the number of edges and N_C the number of vertices. In fact usually n_C and N_C are nearly equal, thus the complexity is in $O(n_C^2)$, as in the case of the currents and varifolds metrics. However, as can be seen from the formulas, more operations are needed in the case of normal cycles; in our experiments the cost of computation of the normal cycle metric and its gradient was approximately six times higher than in the case of currents.

Error of the approximation. We focus here on the error of approximation between $N(C)_{approx}$ previously defined, and $N(C)$, where C is a discretized curve in $\mathbb{R}^d$. More precisely, if we consider a segment S with extremities a and b, and $\omega \in \Omega^{d-1}(\mathbb{R}^d \times S^{d-1})$, we have for the cylindrical part of the original normal cycle:

$$N(S)^{cyl}(\omega) = \int_{(b-a)\times S^{\perp}_{b-a}} \langle \omega(x,n)|(\tau, 0)\wedge \nu(n)\rangle\, d\mathcal{H}^{d-1}(x,n)$$

where $\tau = \frac{b-a}{\|b-a\|}$, and $\nu(n)$ is defined as in Definition 35 (for $v = b - a$).

PROPOSITION 39. *Assume that W is continuously embedded in $\Omega^{d-1}_{1,0}(\mathbb{R}^d \times S^{d-1})$. Then if C is a discretized curve, we have*

$$\|N(C) - N(C)_{approx}\|_{W'} \leq Kl(C)\delta(C)$$

where $l(C) = \mathcal{H}^1(C)$ is the length of C, and $\delta(C)$ is the maximal length of the segments of C. K is a constant.

Proof. We recall that we do not use any approximation on the spherical part and that the cylindrical part and the spherical part are orthogonal with respect to the kernel metric. Thus, to estimate the error, it is sufficient to look at the cylindrical part of the normal cycles involved.

Let $\omega \in \Omega^{d-1}_{1,0}(\mathbb{R}^d \times S^{d-1})$ and $S = [a, b]$ be a single segment. We have:

(20)
$$\begin{aligned}\left|\left(N(S)^{cyl} - N(S)^{cyl}_{approx}\right)(\omega)\right| = \Bigg| &\int_{(b-a)\times S^{\perp}_{b-a}} \langle \omega(x,n)|(\tau,0)\wedge\nu(n)\rangle \, d\mathcal{H}^{d-1}(x,n) \\ &- \int_{S^{\perp}_{b-a}} \langle \omega(c,n)|(b-a,0)\wedge\nu(n)\rangle \, d\mathcal{H}^{d-2}(n)\Bigg| \\ &= \int_{(b-a)\times S^{\perp}_{b-a}} |\langle \omega(x,n) - \omega(c,n)|(\tau,0)\wedge\nu(n)\rangle| \, d\mathcal{H}^{d-1}(x,n)\end{aligned}$$

Since W is assumed to be continuously embedded in the space of $\mathcal{C}^1$ differential forms, then we have $|\omega(x,n) - \omega(c,n)| \leq \|\omega\|_{1,\infty} |x - c| \leq K \|\omega\|_W |c - x|$.

Thus
$$\left|\left(N(S)^{cyl} - N(S)^{cyl}_{approx}\right)(\omega)\right| \leq K' \|\omega\|_W |b-a|^2$$

where K' is a constant taking into account K and the Hausdorff measure of $S^{\perp}_{b-a}$.For the total discretized curve C, we get:

$$\left|\left(N(C)^{cyl} - N(C)^{cyl}_{approx}\right)(\omega)\right| \leq C \|\omega\|_W \, l(C)\delta(C)$$

which proves the result. ∎

4. Curve Matching via Normal Cycles. Given two curves C, S in $\mathbb{R}^3$, we define the curve matching problem as the minimization of a functional over a given set of deformations G. This functional takes the form

$$\varphi_0 = \arg\min_{\varphi \in G} E(\varphi) + A(\varphi.C) \tag{21}$$

where $E(\varphi)$ is an energy term which ensures regularity of the mapping and A is a data attachment term which defines a closeness between the deformed shape $\varphi.C$ and the target shape S (S is fixed). $\varphi.C$ denotes the action of the diffeomorphisms on our shape C.

A coherent framework necessitates a combination of two aspects: a well defined group G with an associated energy E, and a space where our shapes are represented. In our experiments we chose to use the Large Deformation Diffeomorphic Metric Mapping (LDDMM) framework for defining the space G of deformations and the energy E. But of course other frameworks for non-rigid registration could be used, such as for example Thin Plate Splines ([6]). Our shape space will rely on the theory of normal cycles previously developed.

4.1. Large Deformation Diffeomorphic Metric Mapping (LDDMM), continuous case. The idea of LDDMM is close to fluid mechanics: if we consider the evolution of particles along a time varying vector field, the resulting deformation at time one of the system will be obtained by integrating this vector field. And the energy of this deformation is the integration of the infinitesimal cost of displacement of the particles.

It is possible to write it in a more formal way: let $V \hookrightarrow \mathcal{C}_0^1(\mathbb{R}^d, \mathbb{R}^d)$ be a Hilbert of vector fields, whose norm $\|.\|_V$ represents the infinitesimal cost of displacement. Notice here that V is thus a RKHS, with kernel K_V. We define $L_V^2 = \left\{(v_t)_{0\leq t\leq 1} \in V^{[0,1]} | \int_0^1 \|v_t\|_V^2 \, dt < +\infty\right\}$, the set of all time-varying vector fields with finite energy (with respect to the norm on V). The group G_V of diffeomorphisms will be defined as $G_V := \left\{\varphi_1^v, v \in L_V^2\right\}$ with

$$\begin{cases} \dfrac{\partial \varphi_t^v}{\partial t} = v_t \circ \varphi_t^v \\ \varphi_0 = \mathrm{Id} \end{cases}$$

which means that we consider deformations at time one, with finite energy (with respect to the norm V). All this construction has been widely detailed for example in [4], [34], Chap. 8. and following. An exact matching problem between two shapes C and S can then be formulated as follows:

$$\begin{cases} \min\limits_{v\in L^2([0,1],V)} J(v) := \displaystyle\int_0^1 \|v_t\|_V^2 \, dt \\ \dfrac{\partial \varphi_t^v}{\partial t} = v_t \circ \varphi_t^v \\ \varphi_1^v.C = S, \ \varphi_0^v = \mathrm{Id} \end{cases} \tag{22}$$

The LDDMM framework is convenient since we forget the shapes we are working with, and focus our modelling effort on the group G_V. Thus, it can be applied in a wide range of matching problems (images, landmarks, curves, surfaces, etc.). However, the exact matching problem supposes that given two shapes, one can perform a perfect matching. This assumption being unrealistic, we will rather consider the inexact matching problem:

$$\min_{v\in L_V^2} \int_0^1 \|v_t\|_V^2 \, dt + A\left(\varphi_1^v.C, S\right) \tag{23}$$

where A is a dissimilarity measure between the deformed shape $\varphi_1^v.C$ and the target shape S. The next theorem tackles the existence of a solution for (23):

THEOREM 40 ([21]). *If, for every C, S, $v \mapsto A\left(\varphi_1^v.C, S\right)$ is weakly continuous from L_V^2 to $\mathbb{R}$ then (23) has a solution.*

As announced, we will choose A as the kernel metric on normal cycles associated with the shapes S and C :

$$A(C, S) = \|N(C) - N(S)\|_{W'}^2$$

The minimization problem with dual Hilbert norm on normal cycles as data attachment term is then:

$$\min_{v\in L^2_V} \gamma \int_0^1 \|v_t\|_V^2\, dt + \|\varphi^v.N(C) - N(S)\|^2_{W'} \tag{24}$$

where γ is a trade-off parameter. We now state the theorem of existence of a minimizer for (24):

THEOREM 41 (Existence of a minimizer for (24)). *Assume that one has the embeddings $V \hookrightarrow \mathcal{C}^3_0(\mathbb{R}^d, \mathbb{R}^d)$, and $W \hookrightarrow \mathcal{C}^1_0\left(\mathbb{R}^d \times S^{d-1}, \Lambda^{d-1}(\mathbb{R}^d \times \mathbb{R}^d)^*\right)$. Then there exists a minimizer for the problem (24).*

We will prove Theorem 41 using Theorem 40. For this, we have to show that $v \mapsto A(\varphi^v.C, S) = \|\varphi^v.N(C) - N(S)\|^2_{W'}$ is weakly continuous. The first step is to verify that if $v^n \rightharpoonup v$, then $\psi^{v^n} \to \psi^v$ and $d\psi^{v^n} \to d\psi^v$, uniformly on every compact (where the diffeomorphism ψ, representing the deformation of the normal cycle associated with φ, is defined in subsection 1.2.5). We will need the theorem:

THEOREM 42 ([21]). *Suppose that $V \hookrightarrow \mathcal{C}^p_0(\mathbb{R}^d, \mathbb{R}^d)$ (for the topology of uniform convergence for a function and its derivatives). If v^n weakly converges towards v in L^2_V, then $d^k\varphi^{v^n}$ converges uniformly on every compact sets towards $d^k\varphi^v$, $\forall 0 \leq k \leq p-1$.*

From this, we can state the next proposition:

PROPOSITION 43. *Suppose that $V \hookrightarrow \mathcal{C}^3_0(\mathbb{R}^d, \mathbb{R}^d)$. If $v^m \rightharpoonup v$ in L^2_V, then on every compact sets of $\mathbb{R}^d \times S^{d-1}$, $\psi^{v^m} \to \psi^v$, $d\psi^{v^m} \to d\psi^v$*

Proof. If we suppose that $v^m \rightharpoonup v$ in L^2_V, then on every compact sets of $\mathbb{R}^d$, we have: $\varphi^{v^m} \to \varphi^v$, $d\varphi^{v^m} \to d\varphi^v$ and $d^2\varphi^{v^m} \to d^2\varphi^v$ uniformly, with Theorem 42. Now, let K be a compact set of $\mathbb{R}^d$. On K, φ^{v^n} converges uniformly toward φ^v, which proves the uniform convergence for the first component of ψ. For the second component, we consider the application θ:

$$\theta : (A, n) \in GL_d(\mathbb{R}) \times S^{d-1} \mapsto \frac{A^{-t}n}{\|A^{-t}n\|} \in S^{d-1}$$

where the notation A^{-t} stands for $(A^{-1})^t$, the transpose of the inverse. θ is continuous and then is uniformly continuous on every compact sets of $GL_d(\mathbb{R}) \times S^{d-1}$. Moreover,

$$\psi(x, n) = \big(\varphi(x), \quad \theta(d\varphi_x, n)\big)$$

Denoting $d\varphi(K) = \{d\varphi_x | x \in K\}$, $d\varphi(K)$ is a compact of $GL_d(\mathbb{R})$ (the image of a compact by a continuous application is compact) θ is then uniformly continuous on $d\varphi(K) \times S^{d-1}$. Since the uniform convergence is preserved by the composition with a uniformly continuous function, and since $d\varphi^{v^m}$ uniformly converges toward $d\varphi^v$, it proves that the second component of ψ^{v^m} converges uniformly on every compact set of $\mathbb{R}^d \times S^{d-1}$. Which proves that ψ^{v^m} converges uniformly towards ψ^v on every compact sets.

The proof of the uniform convergence of $d\psi^{v^m}$ is similar, using the uniform convergence of $d^2\varphi^{v^m}$. ∎

We recall here a proposition from [21], proposition 34.

PROPOSITION 44. *Let W be a RKHS of m-differential forms continuously embedded in $\Omega^m_{1,0}(\mathbb{R}^d)$. Let S be a m-rectifiable set. If ϕ^n and $d\phi^n$ converge uniformly towards ϕ and $d\phi$ on the support S, then $\phi^n_\sharp S$ converges towards $\phi_\sharp S$ in W'.*

We can now prove Theorem 41:

Proof. Suppose that $v^n \rightharpoonup v$ in L^2_V. By Proposition 43, $\psi^{v^n} \to \psi^v$ and $d\psi^{v^n} \to d\psi^v$. Then, with Proposition 44, and the fact that W is embedded in $\mathcal{C}^1_0\left(\mathbb{R}^d \times S^{d-1}, \Lambda^{d-1}(\mathbb{R}^d \times \mathbb{R}^d)\right)$ we have $\psi^{v^n}_\sharp N(C) \to \psi^v_\sharp N(C)$ in W', which implies that $\left\|\psi^{v^n}_\sharp N(C) - N(S)\right\|^2_{W'} \to \left\|\psi^v_\sharp N(C) - N(S)\right\|^2_{W'}$ and this is exactly the weak continuity of our data attachment term. We conclude using Theorem 40. ∎

In this article, K_V will be a Cauchy kernel, with width σ_V: $K_V(x,y) = \frac{1}{1+\frac{|x-y|^2}{\sigma_V^2}}$, and W is as in Proposition 25. So that we have existence of a minimizer for (24).

Knowing that a minimizer exists is a first step, and we will focus now on the problem to find such a minimizer.

In the next section, we focus on the discrete problem: we consider discrete shapes C_d and S_d. The geodesic equation followed by φ^v_t are simpler and we will explicit the approximations made for the data attachment term in order to have a tractable algorithm for the minimization procedure.

4.2. LDDMM, computational framework. A discrete shape C_d is defined as a set of N points $(x_i)_{1\leq i\leq N}$ in $\mathbb{R}^d$ (the vertices), with a connectivity matrix describing the connexion between the vertices. This applies for curves in $\mathbb{R}^3$ but also for any polyhedral shape in $\mathbb{R}^d$. However, we will restrain our problem to curves in $\mathbb{R}^d$, and we will use the approximation of normal cycles for segments seen in Definition 35 . The functional to minimize is then:

$$J'(v) = \int_0^1 \|v_t\|^2_V \, dt + \|\varphi^v_1.N(C_d)^{approx} - N(S_d)^{approx}\|^2_{W'} \tag{25}$$

However, $\varphi^v_1.N(C_d)^{approx} = \psi^v_{1\sharp}N(C)^{approx}$ is too complex to be implemented numerically. To overcome this difficulty, we approximate the action of φ^v on C_d. For this purpose, we define C_{d,φ^v} as the discrete curve with vertices $(\varphi^v_1(x_i))_{1\leq i\leq N}$ with the same connectivity matrix as C_d. This means that we consider that φ^v induces a displacement of the vertices only, and the displaced vertices are linked with straight lines. From this, we introduce the approximate matching problem, with the functional $\tilde{J}$:

$$\tilde{J}(v) = \int_0^1 \|v_t\|^2_V \, dt + \|N(C_{d,\varphi^v})^{approx} - N(S_d)\|^2_{W'} \tag{26}$$

As shown in [21], if we denote by $q_i(t) = \varphi^v_t(x_i)$ the points trajectories, the energy term in (26) enforces the optimal vector field to be a geodesic path and to write

$$v_t = \sum_{i=1}^N K_V(\cdot, q_i(t))p_i(t) \tag{27}$$

where the $p_i(t) \in \mathbb{R}^d$ are auxiliary variables and are called momentum vectors. Further, it was shown in [26] (and detailed in an optimal control point of view in [1]) that the problem can be written in Hamiltonian form: if we denote H_r the reduced

Hamiltonian:

$$H_r(p(t),q(t)) = \frac{1}{2}\sum_{i=1}^{N}\sum_{j=1}^{N} p_j(t)^T K_V(q_i(t),q_j(t))p_i(t) = \|v_t\|_V^2\,,$$

q_i and p_i must satisfy coupled geodesic equations which write

$$\begin{cases} \dot{q}_i(t) = \displaystyle\sum_{j=1}^{N} K_V(q_i(t),q_j(t))p_j(t) = \frac{\partial H_r}{\partial p_i} \\ \dot{p}_i(t) = -(d_{q_i(t)}v_t)^* p_i(t) = -\dfrac{\partial H_r}{\partial q_i}. \end{cases} \tag{28}$$

This Hamiltonian is constant along geodesic path and thus is a function of the initial momenta p_0 and the initial positions q_0. As could be expected, this implies that the optimal velocity vector field v_t in (27) is of constant norm: $\|v_t\|_V^2 = cste = H_r(q_0,p_0)$. Initial positions being fixed, we can consider H_r and further φ^v as function of the p_0 only φ^{p_0}. The Hamiltonian formalism reduces the initial problem of minimization on an infinite dimensional Hilbert space V (26) to a minimization on $(\mathbb{R}^d)^N$:

$$\min_{p_0\in(\mathbb{R}^d)^N} H_r(p_0,q_0) + \|N(C_{d,\varphi^{p_0}})^{approx} - N(S_d)\|_{W'}^2 \tag{29}$$

and where q and p follow the coupled geodesic (28). The second term depends only on the position of the final vertices: $(q_i(1))_{1\le i\le N} = (\varphi_1^{p_0})_{1\le i\le N}$ that we will denote $q(1)$. The data attachment term is then a function of $q(1)$: $A(q(1))$.

$$\min_{p_0\in(\mathbb{R}^d)^N} J(p_0) := \gamma H_r(p_0,q_0) + A(q(1)) \tag{30}$$

with q and p following (28). As said before, A is a measure of the residual dissimilarity between the deformed shape at time 1 with vertices $q(1)$ and the target shape S_d.

This function can be computed explicitely using the expressions for the scalar products (18), (19). We refer to [26, 1] for an explicit algorithm to minimize (30) with a gradient descent on initial momenta). This algorithm is called geodesic shooting. A numerical implementation of the minimization requires the computation of $\nabla A((x_k)_{1\le k\le N}))$, which takes an explicit form by deriving these expressions. See Appendix E.

5. Application to 3D Curve Matching. In our numerical implementation, we use the shooting algorithm and optimize the functional depending on p_0 with a quasi Newton Broyden Fletcher Goldfarb Shanno algorithm with limited memory (L-BFGS) [23]. The step in the descent direction is fixed by a Wolfe line search. For the numerical integrations, a Runge-Kutta (4,5) scheme is used (function ode45 in Matlab). For the deformation model, we set K_V to be a scalar Cauchy kernel $K_V(x,y) = 1/(1+|x-y|^2/\sigma_V^2)I_d$, with σ_V a scale parameter. For the normal cycles, the point kernel k_p is a Gaussian kernel, with width σ_W, and the normal kernel k_n is a Sobolev kernel, associated with the operator $L = (I-\Delta)^3$. We used a spherical harmonics expansion of this kernel truncated at order 10 for the numerical purpose. We chose to use a weighted scalar product for normal cycles (see Note 24 and Note 37) with weight λ of the form $\lambda = \alpha\sigma_W^2$, where $\alpha > 0$ is a fixed parameter. Setting λ to

be proportional to σ_W^2 comes from a simple homogeneity analysis of the functional (30): when scaling the data coordinates by a factor η, scaling accordingly the width parameters σ_V and σ_W by the same factor, and evaluating at $p_0' = \eta p_0$, the energy term H_r and the cylindrical parts of the scalar products in the normal cycles term are multiplied by η^2, while the spherical part is kept unchanged. Hence multiplying the spherical part by a factor proportional to σ_W^2 ensures homogeneity of the functional with respect to scaling. In all our experiments, we set $\alpha = 10$.

In this section, we show some of our results on synthetic data and compare them with the varifolds method and currents method. The point kernel chosen for the varifolds is a Gaussian kernel, with the same width σ_W as for normal cycles. The kernel associated with the Grassmannian is chosen linear (see [11]), so that no parameter is involved as for the normal kernel with normal cycles. Lastly, a Gaussian kernel is used as well for currents, again with width σ_W. The trade-off parameter γ is set to $\gamma = 0.1$ in all experiments. All the numerical computations have been done on a laptop using Matlab.

Registrations of branching curves (Figure 3). The first example of registration is two 3D curves with branching. These curves were chosen because the distance between them is large compared to their typical sizes, the curves have some high local curvature and the size of the corresponding branches implies high local deformations. Besides, we would like to see the behaviour of normal cycles with respect to connecting points.

The two curves are enclosed in a cubic box of size one. Both curves have 150 vertices. In Figure 3, we show two views of a matching using with normal cycles, varifolds and currents. The kernel K_V associated to the deformation space is chosen to be a Cauchy kernel, with width $\sigma_V = 0.2$. Computation time for registration with currents was 188 seconds (531 iterations of the minimization process, 0.35 second per iteration), 325 seconds for varifolds (874 iterations, 0.37 s/iter), and 832 seconds for normal cycles (1814 iterations, 0.46 s/iter).

Remark 45. As we can notice the computation time per iteration is not increasing much when using normal cycles instead of currents or varifolds. This comes from the fact that the largest part of the computation is spent in solving the ODE equations of the LDDMM shooting procedure. The cost of the data attachment evaluations (functional and gradient) themselves for this experiment reflect the increasing complexity of the methods, as expected: 0.017, 0.036 and 0.10 seconds per iteration for currents, varifolds and normal cycles respectively, but this has relatively small influence on the total time per iteration. In the end, the large total time differences in this experiment come from the number of iterations of the minimization process needed to reach the stopping criterion, which seem to increase with the complexity of the method.

For validation purposes, in order to have a measurement of the closeness between the two matched curves and compare the different registrations, we computed the Hausdorff distance and a mean Hausdorff distance defined as

$$d_s(S, C') = \max\left(\sup_{x \in C'} d(x, S), \sup_{x \in S} d(y, C')\right),$$

$$d_m(S, C') = \frac{1}{\mathcal{H}^1(C') + \mathcal{H}^1(S)}\left(\int_{C'} d(x, S) d\mathcal{H}^1(x) + \int_S d(y, C') d\mathcal{H}^1(y)\right).$$

In practice these quantities were approximated by subsampling each polygonal curve and evaluating all pairwise distances between vertices.

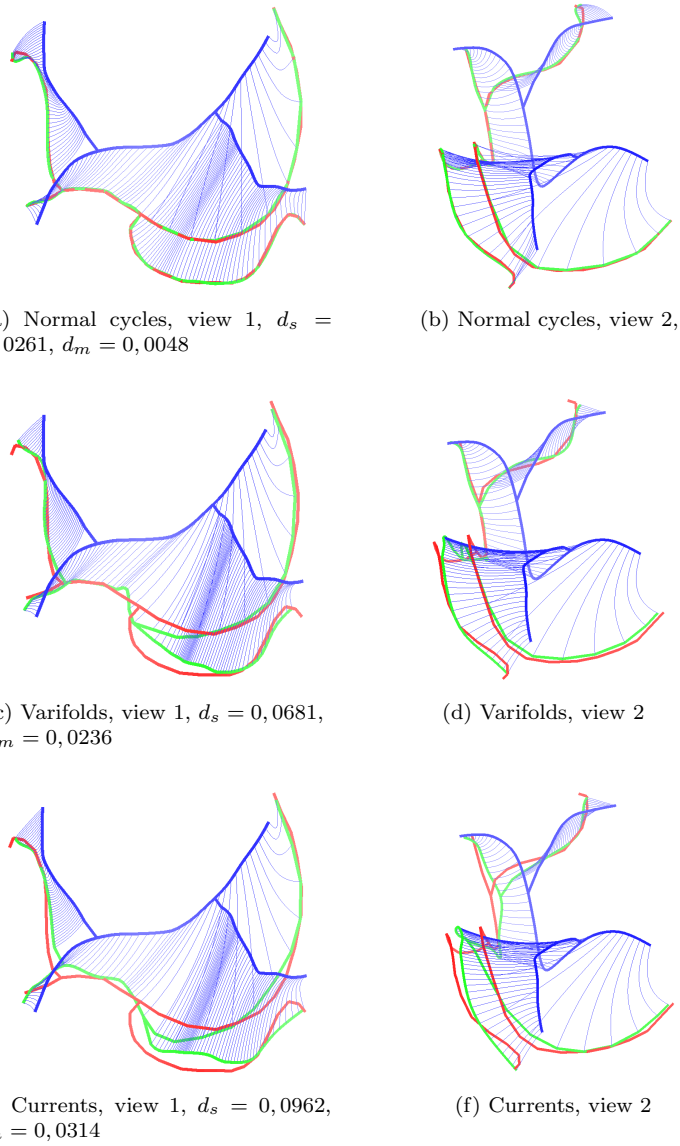

(a) Normal cycles, view 1, $d_s = 0,0261$, $d_m = 0,0048$

(b) Normal cycles, view 2,

(c) Varifolds, view 1, $d_s = 0,0681$, $d_m = 0,0236$

(d) Varifolds, view 2

(e) Currents, view 1, $d_s = 0,0962$, $d_m = 0,0314$

(f) Currents, view 2

FIG. 3. *Registration of two 3D curves with different data attachment terms. Initial curve is in black, target curve in red, and deformed curve in green. Trajectories of vertices along the flow are displayed in blue. Parameters are* $\sigma_V = 0.2$ *and* $\sigma_W = 0.3$

Registration of fishes contours (Figure 4). Here a registration between two fishes contours is performed (see [30] for the original data). Even if they are 2D objects, we consider them as 3D objects with no z variation. In this example, fishes have around 100 vertices. A first optimization of the momenta was performed with parameters $\sigma_W = 0.75$ and $\sigma_V = 0.2$. This can be seen as an initialization step to avoid local minima. Then minimization was done with $\sigma_W = 0.2$ and $\sigma_V = 0.2$. Computation time was 180 seconds for normal cycles (789 iterations, 0.23 s/iter) and 105 seconds for varifolds (582 iterations, 0.18 s/iter). The main difficulty here is the trade off to

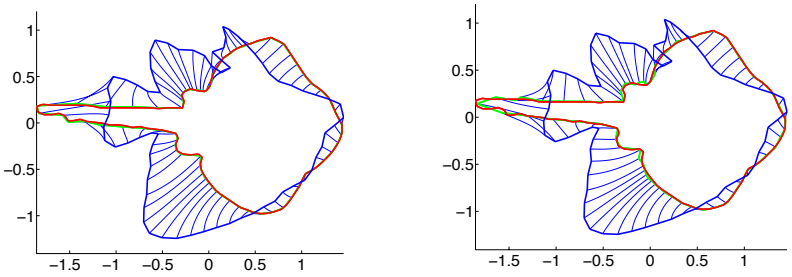

(a) Normal cycles, $d_s = 0,0236$, $d_m = 0,0082$

(b) Varifolds, $d_s = 0,0416$, $d_m = 0,0110$

FIG. 4. *Registration of a dark fish to a red fish. In green the dark deformed fish matching the red one. We used normal cycles and varifolds with the same parameters* $\sigma_V = 0.2$ *and* $\sigma_W = 0.2$. *The registration with currents is worse than with varifolds.*

find between the matching of the long tail of the stingray (in green in Figure 4) and the high local curvature in the upper part of the fish in dark. The results in Figure 4 show that a perfect matching with normal cycles can be achieved, even with $\sigma_W = 0.2$ which is quite large compared to the local feature in the upper part of the fish. With varifolds, one can see that this local feature still remains in the green matched curve. To avoid this behaviour, one can decrease the size of σ_W, but it would lead to a bad matching of the tail.

Registration of brain sulci (Figure 5). We show here an example on real data. The data consist of brain sulcal curves that were automatically segmented and labelled from anatomical Magnetic Resonance Imaging (MRI) brain images, following the method described in [3]. We chose two individuals and six labelled corresponding sulcal curves for each individual. The matching is performed with a single deformation, but 6 data attachment terms with normal cycles: one for each pair of corresponding sulci. Processing times were 29 min using normal cycles (1822 iterations, 1.04 s/iter) and 21 min with varifolds (1559 iterations, 0.82 s/iter). The matching is complex since the number of branching points is not necessarily the same for corresponding curves, and two curves to match can be really twisted from one to another. Moreover, the fact that a single deformation is required for the whole brain implies high local variations. We see in the result that the end points and corresponding branching points are always well matched. Moreover, the registration driven by normal cycles allows complex local deformation (even though it is expensive) to reduce the data attachment term.

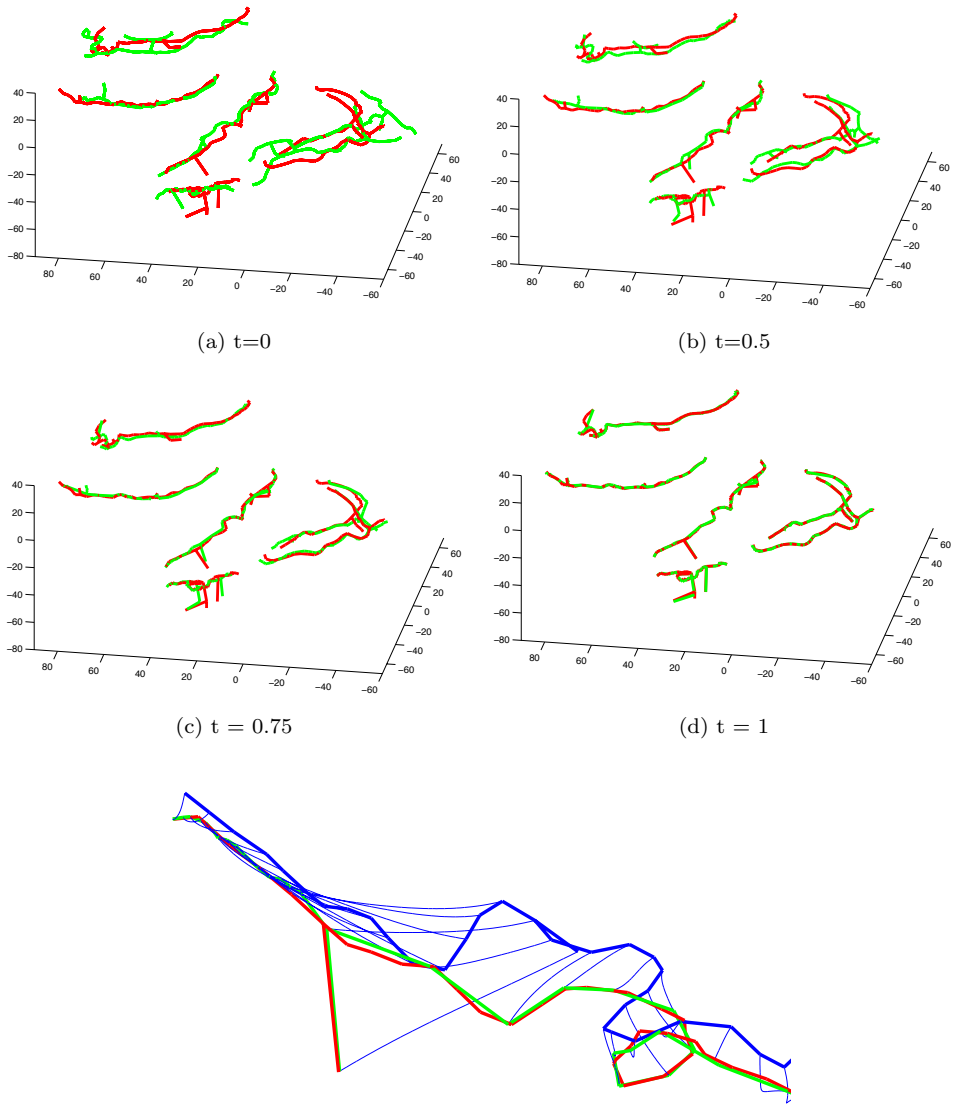

(a) t=0

(b) t=0.5

(c) t = 0.75

(d) t = 1

(e) Zoom

FIG. 5. *Registration of brain sulci of two subjects with normal cycles.* $\sigma_V = 10$ *and* $\sigma_W = 7$. *The size of the kernels are given in mm.* $d_S = 2,90$ $d_m = 0,54$. *The registration has also been done with varifolds with the same parameters and we obtain:* $d_s = 4.46$ *and* $d_m = 0.84$.

In conclusion we have seen that despite an increase of the calculation time, normal cycles improve the matching, especially for branching curves, or curves with end points. We must point out however that these conclusions hold for the particular examples of kernels we chose for the three methods : currents, varifolds and normal cycles. It will be interesting in future experiments to make comparisons with the use of other kernels, for example a gaussian kernel instead of a linear kernel for the varifold metric, as in [9], or other types of kernels for the spherical part in the normal cycle metric. Besides taking into account the curvature of the curves, we believe that another advantage of using normal cycles for the matching of such structures is the "connection cost". Indeed the norm of two segments at distance ε with $\varepsilon \to 0$ is different from the norm of the joint segments, and the difference is exactly the norm of a sphere. This observation is clear when looking at the decomposition of the normal bundle used (Subsection 3.2.1). This cost of connection does not appear for currents or varifolds. More generally, currents and varifolds are m-dimensional measures associated with a m-dimensional objects, and thus are insensitive to the boundaries (which is $m-1$ dimensional). Since normal cycles consider currents associated with the normal bundle, the boundaries are also taken into account during the registration, and are enforced to match as well.

6. Perspectives. In this article, we have presented the first application of normal cycles in the context of 3D curve registration. We have seen that the representation with normal cycle encodes all the curvature information of a shape. As for currents, a kernel metric is used to provide a closed form for the distance between two curves, and a numerical derivation is done for curves approximated by unions of segments. The first results on synthetic data are promising and suggest that normal cycles perform better on connection points and regions with high curvature. Of course, taking into account the curvature can be problematic if the data are noisy. For such problem, a matching with currents would be more efficient. More exhaustive studies on synthetic and real data are necessary to validate this method. The next stage will be the registration using normal cycles for surfaces. This case is more intricate, at least numerically since the decomposition of normal bundle as seen in section 3 is more complex. This brings us to the question of good approximations for normal cycles, in order to reduce the numerical complexity of the matching algorithm. Moreover, the set up of the computational framework for the matching problem made in subsection 4.2 is a first step for the study of the gamma convergence of our discrete problems. We also would like to investigate the link between varifolds and normal cycles, as we believe that varifolds can be seen in our context as a projection of normal cycles, by ignoring variation in S^{d-1}.

Acknowledgments. We thank Guillaume Auzias for extracting and providing us the dataset of sulcal curves used in our experiments.

Appendix A. Spherical Harmonics. The sphericals harmonics are eigenvectors of the spherical Laplacian. In the same spirit as Fourier expansion, spherical harmonics are useful to expand a function on the sphere since they form an orthonormal basis of the Hilbert space $L^2(S^2)$. This basis encodes spatial frequencies on the latitude and the longitude: the first spherical harmonics describe low spatial variation on the sphere, and the more we expand a function on this basis, the more details about the spatial frequencies of this function we get.

Spherical harmonics will be useful in this paper to explicit the normal kernel: since the RKHS we chose on the sphere is a Sobolev Hilbert space, it can be ex-

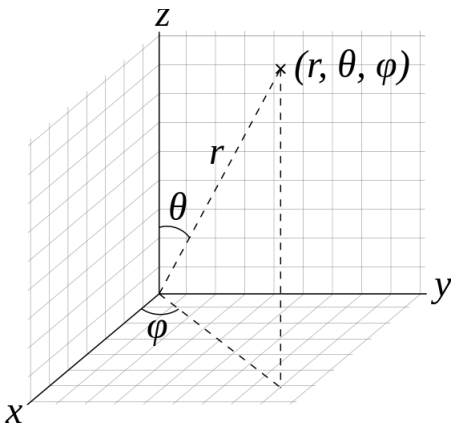

FIG. 6. *Spherical coordinates,* $\varphi \in [0, 2\pi]$ *and* $\theta \in [0, \pi]$

pressed as the RKHS defined by an operator $L_V = (\mathrm{Id} - \Delta)^s$, and the normal kernel will have an explicit expansion.

A scalar function on the unit sphere can be seen as a function of two variables θ, φ, where $\theta \in [0, \pi]$ is the polar angle and $\varphi \in [0, 2\pi]$ the azimuthal angle (see Figure 6)

There are $2l + 1$ spherical harmonics of order l, denoted $(Y_{l,m})_{-l \leq m \leq l}$ and satisfying the equations

$$\begin{cases} -\Delta_{S^2} Y_{l,m}(\theta, \varphi) = l(l+1) Y_{l,m}(\theta, \varphi) \\ -\dfrac{\partial Y_{l,m}}{\partial \varphi} = m Y_{l,m}(\theta, \varphi) \end{cases} \tag{31}$$

The $(Y_{l,m})_{\substack{l \geq 0 \\ -l \leq m \leq l}}$ form an orthonormal basis of $L^2(S^2)$, endowed with its usual scalar product. Thus, any $f \in L^2(S^2)$ can be written

$$f = \sum_{l \geq 0} \sum_{m=-l}^{l} \alpha_{l,m} Y_{l,m}$$

where the limit is in L^2. We have explicit expression of the spherical harmonics with the Legendre polynomials . We will rather use the real spherical harmonics:

$$\begin{cases} Y_{l0}(\theta, \varphi) = \sqrt{\dfrac{2l+1}{4\pi}} P_l(\cos\theta) \\ Y^c_{lm}(\theta, \varphi) = \sqrt{\dfrac{2l+1}{2\pi} \dfrac{(l-m)!}{(l+m)!}} P_l^m(\cos\theta) \cos(m\varphi) \\ Y^s_{lm}(\theta, \varphi) = \sqrt{\dfrac{2l+1}{2\pi} \dfrac{(l-m)!}{(l+m)!}} P_l^m(\cos\theta) \sin(m\varphi) \end{cases} \tag{32}$$

$$P_l(x) = \frac{1}{2^l l!}\frac{d^l}{dx^l}(x^2-1)^l$$
$$= \sum_{\frac{l}{2}\leq k\leq l}(-1)^{l-k}\frac{(2k-1)!!}{(l-k)!(2k-l)!2^{l-k}}x^{2k-l}$$

and

$$P_l^m(x) = (-1)^m(1-x^2)^{m/2}\frac{d^m}{dx^m}P_l(x)$$
$$= (-1)^{l+m}(1-x^2)^{m/2}\sum_{\frac{m+l}{2}\leq k\leq l}(-1)^k\frac{(2k-1)!!}{(l-k)!(2k-(m+l))!2^{l-k}}x^{2k-(m+l)}$$

with $(2n+1)!! = 1*3*\cdots*(2n+1)$ and $(2n)!! = 2*4*\cdots*2n$.

Appendix B. Some Notations.

$$a_{kl} := \int_0^\pi \sin^k\theta\cos^l\theta d\theta = \frac{l-1}{k+1}a_{k+2,l-2}$$

We get obviously with induction:

$$a_{kl} = \begin{cases} 0 & \text{if } l \text{ is odd} \\ \dfrac{2(k-1)!!(l-1)!!(k+l-1)!!}{(k+l)!} & \text{if } l \text{ is even and } k \text{ odd} \\ \dfrac{(l-1)!!(k-1)!!}{(k+l-1)!!}\dfrac{(k+l)!}{(k+l)!!^2}\pi & \text{if } k,l \text{ are even} \end{cases}$$

With these notations, we have:

$$D_{l,0,i,j} = \sqrt{\frac{2l+1}{4\pi}}\int_0^\pi P_l(\cos\theta)\sin^i\theta\cos^j\theta d\theta$$
$$= \sqrt{\frac{2l+1}{4\pi}}\sum_{l/2\leq k\leq l}(-1)^{l-k}\frac{(2k-1)!!}{(l-k)!(2k-l)!2^{l-k}}a_{i,2k-l+j}$$

and

$$D_{l,m,i,j} = \sqrt{\frac{2l+1}{2\pi}\frac{(l-m)!}{(l+m)!}}\int_0^\pi P_{lm}(\cos\theta)\sin^i\theta\cos^j\theta d\theta$$
$$= \sqrt{\frac{2l+1}{2\pi}\frac{(l-m)!}{(l+m)!}}$$
$$\times\sum_{\frac{m+l}{2}\leq k\leq l}\frac{(-1)^{k+l+m}(2k-1)!!}{(l-k)!(2k-(m+l))!2^{l-k}}\int_0^\pi\sin^{m+i}\theta\cos^{2k-m-l+j}\theta d\theta \quad (33)$$
$$= \sqrt{\frac{2l+1}{2\pi}\frac{(l-m)!}{(l+m)!}}\sum_{\frac{m+l}{2}\leq k\leq l}\frac{(-1)^{k+l+m}(2k-1)!!}{(l-k)!(2k-(m+l))!2^{l-k}}a_{m+i,2k-m-l+j}$$

Appendix C. Computing the scalar product between cylindrical parts (18).

We compute here the approximate scalar product between the cylindrical parts of two segments, C_1 and S_1. $C_1 = [c_0, c_1]$ and $S_1 = [s_0, s_1]$. We use the same notations as in subsection 3.2.1 If we denote $\alpha = \frac{c_1 - c_0}{\|c_1 - c_0\|}$ and $\beta = \frac{s_1 - s_0}{\|s_1 - s_0\|}$ (notice that for every $x \in C_1$, $y \in S_1$, $\tau_{C_1}(x) = \alpha$ and $\tau_{S_1}(y) = \beta$) we have:

$$\left\langle N(C_1)^{cyl}_{approx}, N(S_1)^{cyl}_{approx} \right\rangle_{W'} = \left\langle \delta_{\frac{c_0+c_1}{2}, \alpha^\perp}, \delta_{\frac{s_0+s_1}{2}, \beta^\perp} \right\rangle_{W'}$$

and we can sum up the scalar product:

(34)
$$\left\langle N(C_1)^{cyl}_{approx}, N(S_1)^{cyl}_{approx} \right\rangle = \left\{ k_p \left(\frac{c_0 + c_1}{2}, \frac{s_0 + s_1}{2} \right) \langle c_1 - c_0, s_1 - s_0 \rangle \right\} \times \left\{ \int_{S^\perp_\alpha} \int_{S^\perp_\beta} k_n(u, v) \left\langle \tau_{S^\perp_\alpha}(u), \tau_{S^\perp_\beta}(v) \right\rangle d\mathcal{H}^1(u) d\mathcal{H}^1(v) \right\}$$

The first factor necessitates only the evaluation of the point kernel at the middle of the segments. The second factor is more involved: we will use the expansion on spherical harmonics of the normal kernel developed in subsection 2.4.

A first and very important remark is the future use of the invariance of the normal kernel under a rotation. This means that, if $u, v \in S^2$, $k_n(u, v)$ depends *only* of the relative position of u and v. And by invariance of the kernel, we can suppose that $\alpha = (1, 0, 0)$ and $\beta = (\cos\varphi, \sin\varphi, 0)$ where $\varphi \in [0, \pi]$ is the unoriented angle between α and β (the notations were defined in Figure 6). We will now formulate the integral with the parametrization of the sphere (φ, θ). One should be cautious that the tangent vector $\tau_C(x)$ should have a coherent orientation with α and u, i.e. $\tau_{S^\perp_\alpha}(u) = -\alpha \wedge u$, with $u = \begin{pmatrix} \sin\theta_u \cos\varphi_u \\ \sin\theta_u \sin\varphi_u \\ \cos\theta_u \end{pmatrix}$, and $\tau_{S^\perp_\beta}(v) = -\beta \wedge v$, with $v = \begin{pmatrix} \sin\theta_v \cos\varphi_v \\ \sin\theta_v \sin\varphi_v \\ \cos\theta_v \end{pmatrix}$. u should describe all $S^\perp_\alpha$, which means $\varphi_u = \pm\frac{\pi}{2}$, $\theta_u \in [0, \pi]$ and v should describe all $S^\perp_\beta$, which means $\varphi_v = \pm\frac{\pi}{2} + \varphi$, $\theta_v \in [0, \pi]$. Then, we get

(35)
$$\left\langle N(C_1)^{cyl}_{approx}, N(S_1)^{cyl}_{approx} \right\rangle_{W'} = k_p \left(\frac{c_0 + c_1}{2}, \frac{s_0 + s_1}{2} \right) \langle c_1 - c_0, s_1 - s_0 \rangle$$
$$\sum_{\varphi_u = \pm\frac{\pi}{2}} \sum_{\substack{\varphi_v \\ = \varphi \pm \frac{\pi}{2}}} \int_0^\pi \int_0^\pi k_n(u, v) (\cos\varphi \cos\theta_v \cos\theta_u + \sin\theta_u \sin\varphi_u \sin\theta_v \sin(\varphi_v - \varphi)) d\theta_u d\theta_v$$

Developing k_n in spherical harmonics (see formula (15) ; here we denote $\lambda_l = (1 +$

$l(l+1))^s$), and regrouping the terms, leads to:

$$\begin{aligned}\left\langle N(C_1)^{cyl}_{approx}, N(S_1)^{cyl}_{approx}\right\rangle_{W'} = k_p\left(\frac{c_0+c_1}{2}, \frac{s_0+s_1}{2}\right)\langle c_1-c_0, s_1-s_0\rangle \sum_{\varphi_u=\pm\frac{\pi}{2}} \sum_{\substack{\varphi_v \\ =\varphi\pm\frac{\pi}{2}}} \\ \sum_{l\geq 0}\frac{1}{\lambda_l}\left\{\int_0^\pi Y_{l0}(x)\cos\theta_u d\theta_u \int_0^\pi Y_{l0}(y)\cos\theta_v d\theta_v \cos\varphi\right. \\ + \int_0^\pi Y_{l0}(x)\sin\theta_u d\theta_u \int_0^\pi Y_{l0}(y)\sin\theta_v d\theta_v \sin\varphi_u \sin(\varphi_v-\varphi) \\ + \sum_{m=1}^{l}\int_0^\pi Y^c_{lm}(x)\cos\theta_u d\theta_u \int_0^\pi Y^c_{lm}(y)\cos\theta_v d\theta_v \cos\varphi \\ + \int_0^\pi Y^c_{lm}(x)\sin\theta_u d\theta_u \int_0^\pi Y^c_{lm}(y)\sin\theta_v d\theta_v \sin\varphi_u \sin(\varphi_v-\varphi) \\ + \sum_{m=1}^{l}\int_0^\pi Y^s_{lm}(x)\cos\theta_u d\theta_u \int_0^\pi Y^s_{lm}(y)\cos\theta_v d\theta_v \cos\varphi \\ \left. + \int_0^\pi Y^s_{lm}(x)\sin\theta_u d\theta_u \int_0^\pi Y^s_{lm}(y)\sin\theta_v d\theta_v \sin\varphi_u \sin(\varphi_v-\varphi)\right\}\end{aligned}$$

Using the notations of Appendix B, we get:

$$\begin{aligned}\left\langle N(C_1)^{cyl}_{approx}, N(S_1)^{cyl}_{approx}\right\rangle_{W'} = k_p\left(\frac{c_0+c_1}{2}, \frac{s_0+s_1}{2}\right)\langle c_1-c_0, s_1-s_0\rangle \sum_{\varphi_u=\pm\frac{\pi}{2}} \sum_{\substack{\varphi_v \\ =\varphi\pm\frac{\pi}{2}}} \\ \sum_{l\geq 0}\frac{1}{\lambda_l}\left\{D^2_{l,0,0,1}\cos\varphi + D^2_{l,0,1,0}\sin\varphi_u\sin(\varphi_v-\varphi)\right. \\ + \sum_{m=1}^{l} D^2_{l,m,0,1}\cos\varphi\cos(m(\varphi_u-\varphi_v)) \\ \left. + \sum_{m=1}^{l} D^2_{l,m,1,0}\cos(m(\varphi_u-\varphi_v))\sin\varphi_u\sin(\varphi_v-\varphi)\right\}\end{aligned}$$

Since

$$\sum_{\varphi_u\in\{\pm\frac{\pi}{2}\}}\sum_{\varphi_v\in\{\varphi\pm\frac{\pi}{2}\}}\cos\varphi\cos(m(\varphi_u-\varphi_v)) = \begin{cases}0 & \text{if } m \text{ odd}\\ 4\cos\varphi\cos(m\varphi) & \text{if } m \text{ even}\end{cases}$$

and

$$\sum_{\varphi_u\in\{\pm\frac{\pi}{2}\}}\sum_{\varphi_v\in\{\varphi\pm\frac{\pi}{2}\}}\sin\varphi_u\sin(\varphi_v-\varphi)\cos(m(\varphi_u-\varphi_v)) = \begin{cases}0 & \text{if } m \text{ even}\\ 4\cos(m\varphi) & \text{if } m \text{ odd}\end{cases}$$

We gather the terms and get

$$\begin{aligned}\left\langle N(C_1)^{cyl}_{approx}, N(S_1)^{cyl}_{approx}\right\rangle_{W'} &= k_p\left(\frac{c_0+c_1}{2}, \frac{s_0+s_1}{2}\right)\langle c_1-c_0, s_1-s_0\rangle \\ &\times \sum_{l\geq 0}\frac{1}{\lambda_l}\{(4D^2_{l,0,0,1}+2D^2_{l,2,0,1}+4D^2_{l,1,1,0})\cos\varphi \\ &+ \sum_{\substack{m=3\\ m \text{ odd}}}^{l}\left[4D^2_{l,m,1,0}+2D^2_{l,m-1,0,1}+2D^2_{l,m+1,0,1}\right]\cos(m\varphi)\}\end{aligned}$$

Interverting the summation symbols, we obtain

$$\begin{aligned}\left\langle N(C_1)^{cyl}_{approx}, N(S_1)^{cyl}_{approx}\right\rangle_{W'} &= k_p\left(\frac{c_0+c_1}{2}, \frac{s_0+s_1}{2}\right) \\ &\times \langle c_1-c_0, s_1-s_0\rangle \sum_{m\geq 0} a_m\cos(m\varphi)\end{aligned} \tag{36}$$

with

$$\begin{cases} a_1 = \displaystyle\sum_{l\geq 0}\frac{1}{\lambda_l}(4D^2_{l,0,0,1}+2D^2_{l,2,0,1}+4D^2_{l,1,1,0}) \\ a_{2m-1} = \displaystyle\sum_{l\geq 2m-1}\frac{1}{\lambda_l}(4D^2_{l,2m-1,1,0}+2D^2_{l,2m-2,0,1}+2D^2_{l,2m,0,1}) \\ a_{2m} = 0 \end{cases}$$

Appendix D. Computing the scalar product between the spherical parts. This computation is somehow similar to the previous one. However, one should be cautious at the different terms involved in the computation. As seen in (17), there are different objects in the spherical scalar product: the half sphere, associated with the extremities of the segments, and the sphere, associated with the vertices. Thus the scalar product involves cross terms. We begin with the scalar product between two spheres, i.e. the normal cycles associated with isolated vertices a and b. One should be cautious when parametrizing the integral, as the volume element on the sphere is non trivial.

$$\begin{aligned}\langle N(\{a\}), N(\{b\})\rangle_{W'} =& k_p(a,b)\int_0^{2\pi}\int_0^{\pi} \\ &\left\{\int_0^{2\pi}\int_0^{\pi} k_n(u,v)(\sin\theta_u\sin\theta_v\cos(\varphi_u-\varphi_v)+\cos\theta_u\cos\theta_v)\sin\theta_v d\varphi_v d\theta_v\right\}\sin\theta_u d\varphi_u d\theta_u\end{aligned}$$

With an expansion on spherical harmonics of k_n:

$$\begin{aligned}
\langle N(\{a\}), N(\{b\})\rangle_{W'} &= k_p(a,b)\int_0^{2\pi}\int_0^{\pi}\Bigg\{\int_0^{2\pi}\int_0^{\pi}\sum_{l\geq 0}\frac{1}{\lambda_l}\big(Y_{l0}(x)Y_{l0}(y)\\
&\quad+\sum_{m=1}^{l}Y_{lm}^c(x)Y_{lm}^c(y)+Y_{lm}^s(x)Y_{lm}^s(y)\big)\\
&\times\big(\sin\theta_u\sin\theta_v\cos(\varphi_u-\varphi_v)+\cos\theta_u\cos\theta_v\big)\sin\theta_v d\theta_v d\varphi_v\Bigg\}\sin\theta_u d\theta_u d\varphi_u\\
&= k_p(a,b)\sum_{l\geq 0}\frac{1}{\lambda_l}\big(4\pi^2 D_{l,0,1,1}^2\\
&+\int_0^{2\pi}\int_0^{\pi}Y_{l,1}^c(x)\sin^2\theta_u d\theta_u\int_0^{2\pi}\int_0^{\pi}Y_{l,1}^c(y)\sin^2\theta_v\cos(\varphi_u-\varphi_v)d\varphi_u d\theta_v d\varphi_v\\
&+\underbrace{\int_0^{2\pi}\int_0^{\pi}Y_{l,1}^c(x)\sin\theta_u\cos\theta_u d\theta_u\int_0^{2\pi}\int_0^{\pi}Y_{l,1}^c(y)\sin\theta_v\cos\theta_v d\varphi_u d\theta_v d\varphi_v}_{=0}\\
&+\int_0^{2\pi}\int_0^{\pi}Y_{l,1}^s(x)\sin^2\theta_u d\theta_u\int_0^{2\pi}\int_0^{\pi}Y_{l,1}^s(y)\sin^2\theta_v\cos(\varphi_u-\varphi_v)d\varphi_u d\theta_v d\varphi_v\\
&+\underbrace{\int_0^{2\pi}\int_0^{\pi}Y_{l,1}^s(x)\sin\theta_u\cos\theta_u d\theta_u\int_0^{2\pi}\int_0^{\pi}Y_{l,1}^s(y)\sin\theta_v\cos\theta_v d\varphi_u d\theta_v d\varphi_v}_{=0}\big)
\end{aligned}$$

The integral of the variables φ_u et φ_v cancels all the other terms:

$$\int_0^{2\pi}\int_0^{2\pi}\cos(m\varphi_u)\cos(m\varphi_v)\cos(\varphi_u-\varphi_v)d\varphi_u d\varphi_v=0,\ \ \forall m\geq 2$$

and for $m=1$,

$$\begin{aligned}
&\int_0^{2\pi}\int_0^{2\pi}\cos(\varphi_u)\cos(\varphi_v)\cos(\varphi_u-\varphi_v)d\varphi_u d\varphi_v=\pi\int_0^{2\pi}\cos^2\varphi_v d\varphi_v=\pi^2\\
&=\int_0^{2\pi}\int_0^{2\pi}\sin(\varphi_u)\sin(\varphi_v)\cos(\varphi_u-\varphi_v)d\varphi_u d\varphi_v
\end{aligned}$$

With the same computation as in Appendix C we get:

$$\langle N(\{a\}), N(\{b\})\rangle_{W'} = k_p(a,b)\sum_{l\geq 0}\frac{1}{\lambda_l}\big(4\pi^2 D_{l,0,1,1}^2+2\pi^2 D_{l,1,2,0}^2\big) \tag{37}$$

The scalar product between a half-sphere S_α^+ at point a, and a sphere follows the exact same computation and we get:

$$\big\langle[\{a\}\times S_\alpha^+], N(\{b\})\big\rangle_{W'} = k_p(a,b)\sum_{l\geq 0}\frac{\pi}{\lambda_l}\big(2\pi D_{l,0,1,1}^2+\pi D_{l,1,2,0}^2\big) \tag{38}$$

For the scalar product between two half spheres, S_α^+ and S_β^+ at points a and b:

$$\Big\langle[\{a\}\times S_\alpha^+],[\{b\}\times S_\beta^+]\Big\rangle_{W'} = k_p(a,b)I(\alpha,\beta)$$

where

$$I(\alpha,\beta) = \int_0^{\pi}\int_{-\frac{\pi}{2}}^{\frac{\pi}{2}} \Big\{ \int_0^{\pi}\int_{\varphi-\frac{\pi}{2}}^{\varphi+\frac{\pi}{2}} k_n(u,v)(\sin\theta_u\sin\theta_v\cos(\varphi_u-\varphi_v) + \cos\theta_u\cos\theta_v)\sin\theta_v d\varphi_v d\theta_v \Big\}\sin\theta_u d\varphi_u d\theta_u$$

Again, with an expansion on spherical harmonics:

$$I(\alpha,\beta) = \sum_{l\geq 0}\frac{1}{\lambda_l}\int_{-\frac{\pi}{2}}^{\frac{\pi}{2}}\int_0^{\pi}\int_{\varphi-\frac{\pi}{2}}^{\varphi+\frac{\pi}{2}}\int_0^{\pi}\big(Y_{l0}(x)Y_{l0}(y) + \sum_{m=1}^{l} Y_{lm}(x)Y_{lm}(y)\big) [\sin\theta_u\sin\theta_v\cos(\varphi_u-\varphi_v) + \cos\theta_u\cos\theta_v]\sin\theta_v\sin\theta_u d\theta_v d\varphi_v d\theta_u d\varphi_u$$

Integration on θ_u and θ_v gives (with notations of Appendix B):

$$\begin{aligned} I(\alpha,\beta) = \sum_{l\geq 0}\frac{1}{\lambda_l}\Bigg\{ & D^2_{l,0,2,0}\underbrace{\int_{\frac{-\pi}{2}}^{\frac{\pi}{2}}\int_{\varphi-\frac{\pi}{2}}^{\varphi+\frac{\pi}{2}}\cos(\varphi_u-\varphi_v)d\varphi_v d\varphi_u}_{=4\cos\varphi} + \pi^2 D^2_{l,0,1,1} \\ & + \sum_{m=1}^{l} D^2_{l,m,1,1}\int_{-\frac{\pi}{2}}^{\frac{\pi}{2}}\int_{\varphi-\frac{\pi}{2}}^{\varphi+\frac{\pi}{2}}\big(\cos(m\varphi_u)\cos(m\varphi_v)+\sin(m\varphi_u)\sin(m\varphi_v)\big)d\varphi_v d\varphi_u \\ & + \sum_{m=1}^{l} D^2_{l,m,2,0}\int_{-\frac{\pi}{2}}^{\frac{\pi}{2}}\int_{\varphi-\frac{\pi}{2}}^{\varphi+\frac{\pi}{2}}\big(\cos(m\varphi_u)\cos(m\varphi_v)+\sin(m\varphi_u)\sin(m\varphi_v)\big) \\ & \cos(\varphi_u-\varphi_v)d\varphi_v d\varphi_u \Bigg\} \end{aligned}$$

$$I(\alpha,\beta) = \sum_{l\geq 0}\frac{1}{\lambda_l}\left\{ 4D^2_{l,0,2,0}\cos\varphi + \pi^2 D^2_{l,0,1,1} + \frac{\pi^2}{2}D^2_{l,1,2,0} + \sum_{\substack{m=1\\ m\text{ odd}}}^{l}\frac{4D^2_{l,m,1,1}}{m^2}\cos(m\varphi) + \sum_{\substack{m=1\\ m\text{ even}}}^{l} D^2_{l,m,2,0}\left[\frac{2}{(m-1)^2}\cos((m-1)\varphi) + \frac{2}{(m+1)^2}\cos((m+1)\varphi)\right]\right\}$$

We can write:

$$\begin{aligned} I(\alpha,\beta) &= \sum_{l\geq 0}\frac{1}{\lambda_l}\sum_{m=0}^{l} a_{l,m}\cos(m\varphi) \\ &= \sum_{m\geq 0}\left(\sum_{l\geq m} a_{l,m}\right)\cos(m\varphi) \end{aligned}$$

So

$$\Big\langle [\{a\}\times S^+_\alpha], [\{b\}\times S^+_\beta]\Big\rangle_{W'} = k_p(a,b)\sum_{m\geq 0} b_m\cos(m\varphi) \tag{39}$$

where $b_m = \sum_{l \geq m} a_{l,m}$ with

$$\begin{cases} b_0 = \displaystyle\sum_{l\geq 0} \frac{\pi^2 D^2_{l,0,1,1}}{\lambda_l} + \sum_{l\geq 1} \frac{\pi^2}{2\lambda_l} D^2_{l,1,2,0} \\ b_1 = \displaystyle\sum_{l\geq 0} \frac{4D^2_{l+1,1,1,1}}{\lambda_{l+1}} + \frac{4D^2_{l,0,2,0}}{\lambda_l} + \frac{2D^2_{l+2,2,2,0}}{\lambda_{l+2}} \\ b_m = \displaystyle\frac{1}{m^2} \sum_{l\geq m} \frac{4D^2_{l,m,1,1}}{\lambda_l} + \frac{2D^2_{l-1,m-1,2,0}}{\lambda_{l-1}} + \frac{2D^2_{l+1,m+1,2,0}}{\lambda_{l+1}} \qquad \text{if } m \text{ odd }, m > 1 \\ b_m = 0 \qquad \text{if } m \text{ even }, m > 0 \end{cases}$$

Appendix E. Computing the Gradient of the Norm Associated with a Kernel Metric on Normal Cycles.

Here, we compute in the discrete case the gradient of the cylindrical part of the kernel metric on normal cycles.

$$\begin{aligned} A^{cyl}(C_1, C_2) &:= \left\| N(C_1)^{cyl} - N(C_2)^{cyl} \right\|^2 \\ &= \left\| N(C_1)^{cyl} \right\|^2 + \left\| N(C_2)^{cyl} \right\|^2 - 2 \left\langle N(C_1)^{cyl}, N(C_2)^{cyl} \right\rangle \end{aligned}$$

If we keep the same notations as in the previous appendixes, with

$$\theta_{ij} = \arccos\left(\left\langle \frac{f_i}{|f_i|}, \frac{f_j}{|f_j|} \right\rangle \right),$$

we have (by composing the differentiation):

$$\partial_{x_k} A^{cyl} = \sum_{i=1}^{n} \partial_{p_i} A^{cyl} \circ \partial_{x_k} p_i + \partial_{x_{f_i^1}} A^{cyl} \circ \partial_{x_k} x_{f_i^1} + \partial_{x_{f_i^2}} A^{cyl} \circ \partial_{x_k} x_{f_i^2}$$

with

$$\begin{aligned} \partial_{p_i} A^{cyl} = &\sum_{j=1}^{n} (\partial_1 k_p(p_i, p_j) + \partial_2 k_p(p_j, p_i)) \langle f_i, f_j \rangle \sum_{m\geq 0} a_m \cos(m\theta_{ij}) \\ &- 2 \sum_{j=1}^{m} \partial_1 k_p(p_i, q_j) \langle f_i, g_j \rangle \sum_{m\geq 0} a_m \cos(m\varphi_{ij}) \end{aligned}$$

$$\begin{aligned} \partial_{f_i^2} A^{cyl} = &\, 2 \left(\sum_{j=1}^{n} k_p(p_i, p_j) \sum_{m\geq 0} a_m \cos(m\theta_{ij}) f_j - \sum_{j=1}^{m} k_p(p_i, q_j) \sum_{m\geq 0} a_m \cos(m\varphi_{ij}) g_j \right) \\ &+ 2 \left(\sum_{j=1}^{n} k_p(p_i, p_j) \langle f_i, f_j \rangle \sum_{m\geq 0} \delta_{i\neq j} \frac{m \sin(m\theta_{ij})}{|\sin(\theta_{ij})|} \frac{1}{|f_j|} \left(\frac{f_j}{|f_i|} - \left\langle \frac{f_i}{|f_i|}, \frac{f_j}{|f_i|} \right\rangle \frac{f_i}{|f_i|} \right) \right. \\ &\left. - \sum_{j=1}^{m} k_p(p_i, q_j) \langle f_i, g_j \rangle \sum_{m\geq 0} a_m \frac{m \sin(m\varphi_{ij})}{|\sin(\varphi_{ij})|} \frac{1}{|g_j|} \left(\frac{g_j}{|f_i|} - \left\langle \frac{f_i}{|f_i|}, \frac{g_j}{|f_i|} \right\rangle \frac{f_i}{|f_i|} \right) \right) \end{aligned}$$

here, we use:

$$\begin{aligned}\partial_{f_i^2}\cos(m\varphi_{ij}) &= \frac{m\sin(m\varphi_{ij})}{|\sin(\varphi_{ij})|}\nabla_{f_i^2}\left\langle\frac{f_i}{|f_i|},\frac{g_j}{|g_j|}\right\rangle\\ &= \frac{m\sin(m\varphi_{ij})}{|\sin(\varphi_{ij})|}\frac{1}{|f_i|}\left(\frac{g_j}{|g_j|}-\left\langle\frac{f_i}{|f_i|},\frac{g_j}{|g_j|}\right\rangle\frac{f_i}{|f_i|}\right)\\ &= \frac{m\sin(m\varphi_{ij})}{|\sin(\varphi_{ij})|}\frac{1}{|f_i|}p_{f_i^\perp}\frac{g_j}{|g_j|}\end{aligned}$$

with $p_{f_i^\perp}$ the orthogonal projection on $f_i^\perp$, and

$$\begin{cases}\partial_{x_k}p_i = \frac{1}{2}\left(\delta_{\{k=f_i^1\}}+\delta_{\{k=f_i^2\}}\right)\mathrm{Id}\\ \partial_{x_k}x_{f_i^1} = \delta_{\{k=f_i^1\}}\mathrm{Id}\end{cases}$$

Then, we get for the gradient of A^{cyl}:

$$\begin{aligned}\nabla A^{cyl}((x_k)_{1\le k\le N}) = \Bigg[&\sum_{i=1}^n\left(\sum_{j=1}^n(\nabla_1 k_p(p_i,p_j)+\nabla_2 k_p(p_j,p_i))\langle f_i,f_j\rangle\sum_{m\ge0}\alpha_m\cos(m\theta_{ij})\right.\\ &\left.-2\sum_{j=1}^m\nabla_1 k_p(p_i,q_j)\langle f_i,g_j\rangle\sum_{m\ge0}a_m\cos(m\varphi_{ij})\right)\frac{1}{2}(\delta_{\{k=f_i^1\}}+\delta_{\{k=f_i^2\}})\\ &+2\sum_{i=1}^n\left(\sum_{j=1}^n k_p(p_i,p_j)\sum_{m\ge0}a_m\cos(m\theta_{ij})f_j-\sum_{j=1}^m k_p(p_i,q_j)\sum_{m\ge0}a_m\cos(m\varphi_{ij})g_j\right)\\ &\times(\delta_{\{k=f_i^2\}}-\delta_{\{k=f_i^1\}})\\ &+2\sum_{i=1}^n\left(\sum_{j=1}^n k_p(p_i,p_j)\langle f_i,f_j\rangle\sum_{m\ge0}\delta_{i\ne j}a_m\frac{m\sin(m\theta_{ij})}{|\sin(\theta_{ij})|}\frac{1}{|f_i|}p_{f_i^\perp}\frac{f_j}{|f_j|}\right.\\ &\left.-\sum_{j=1}^m k_p(p_i,q_j)\langle f_i,g_j\rangle\sum_{m\ge0}a_m\frac{m\sin(m\varphi_{ij})}{|\sin(\varphi_{ij})|}\frac{1}{|f_i|}p_{f_i^\perp}\frac{g_j}{|g_j|}\right)\\ &\times(\delta_{\{k=f_i^2\}}-\delta_{\{k=f_i^1\}})\Bigg]_{1\le k\le N}\end{aligned}$$

One can check that $\nabla A^{cyl}((x_k)_{1\le k\le N})\in(\mathbb{R}^3)^N$

With the same type of computation, which we do not detail here, we get also the

gradient for the spherical part:

$$
\begin{aligned}
\nabla A^{sph}((x_k)_{1\leq k\leq N}) = \Bigg(& \sum_{l=1}^{N} (\nabla_1 k_p(x_k, x_l) + \nabla_2 k_p(x_l, x_k)) \Bigg[\left(1 - \frac{n_{x_k} + n_{x_l}}{2}\right) K \\
& + \sum_{i=1}^{n}\sum_{j=1}^{m} (\delta_{\{k=f_i^1\}} - \delta_{\{k=f_i^2\}})(\delta_{\{l=f_j^1\}} - \delta_{\{l=f_j^2\}}) \sum_{m\geq 0} b_m \cos(m\theta_{ij}) \Bigg] \\
& - 2 \sum_{l=1}^{M} \nabla_1 k_p(x_k, y_l) \Bigg[\left(1 - \frac{n_{x_k} + n_{y_l}}{2}\right) K \\
& + \sum_{i=1}^{n}\sum_{j=1}^{m} (\delta_{\{k=f_i^1\}} - \delta_{\{k=f_i^2\}})(\delta_{\{l=g_j^1\}} - \delta_{\{l=g_j^2\}}) \sum_{m\geq 0} b_m \cos(m\varphi_{ij}) \Bigg] \\
+ 2 \sum_{\substack{s \text{ vertex} \\ \text{linked to } k}} & \sum_{l=1}^{N} k_p(x_s, x_l) \sum_{i=1}^{n}\sum_{j=1}^{m} (2\delta_{k=s} - 1)(\delta_{\{l=f_j^2\}} - \delta_{\{l=f_j^1\}})(\delta_{\{s=f_i^1\}} + \delta_{\{s=f_i^2\}}) \\
& \times \sum_{m\geq 1} b_m \frac{m \sin(m\theta_{ij})}{|\sin(\theta_{ij})|} \frac{1}{|f_i|} p_{f_i^\perp} \frac{g_j}{|g_j|} \\
- 2 \sum_{\substack{s \text{ vertex} \\ \text{linked to } k}} & \sum_{l=1}^{M} k_p(x_s, y_l) \sum_{i=1}^{n}\sum_{j=1}^{m} (2\delta_{k=s} - 1)(\delta_{\{l=g_j^2\}} - \delta_{\{l=g_j^1\}})(\delta_{\{s=f_i^1\}} + \delta_{\{s=f_i^2\}}) \\
& \times \sum_{m\geq 0} b_m \frac{m \sin(m\varphi_{ij})}{|\sin(\varphi_{ij})|} \frac{1}{|f_i|} p_{f_i^\perp} \frac{g_j}{|g_j|} \Bigg)_{1\leq k\leq N}
\end{aligned}
$$

REFERENCES

[1] S. Arguillère, E. Trélat, A. Trouvé, and L. Younès, *Shape deformation analysis from the optimal control viewpoint*, Journal de Mathmatiques Pures et Appliques, 104 (2015), pp. 139 – 178.

[2] N. Aronszajn, *Theory of reproducing kernels*, Transactions of the American Mathematical Society, 68 (1950), pp. 337–404.

[3] G. Auzias, O. Colliot, J. A. Glaunes, M. Perrot, J. F. Mangin, A. Trouve, and S. Baillet, *Diffeomorphic brain registration under exhaustive sulcal constraints*, IEEE Transactions on Medical Imaging, 30 (2011), pp. 1214–1227, doi:10.1109/TMI.2011.2108665.

[4] M. F. Beg, M. I. Miller, A. Trouvé, and L. Younes, *Computing Large Deformation Metric Mappings via Geodesic Flows of Diffeomorphisms*, International Journal of Computer Vision, 61 (2005), pp. 139–157.

[5] A. Bernig, *On some aspects of curvature*.

[6] F. L. Bookstein, *Principal Warps: Thin-Plate Splines and the Decomposition of Deformations*, IEEE Transactions on Pattern Analysis and Machine Intelligence, 11 (1989), pp. 567–585.

[7] H. Brézis, *Functional analysis, Sobolev spaces and partial differential equations*, Universitext, Springer, 2011.

[8] C. Carmeli, E. De Vito, A. Toigo, and V. Umanit, *Vector valued reproducing kernel Hilbert spaces and universality*, arXiv:0807.1659 [math], (2008).

[9] B. Charlier, N. Charon, and A. Trouvé, *The fshape framework for the variability analysis of functional shapes*, Foundations of Computational Mathematics, (2015), pp. 1–71, doi:10.1007/s10208-015-9288-2, http://dx.doi.org/10.1007/s10208-015-9288-2.

[10] B. Charlier, G. Nardi, and A. Trouvé, *The matching problem between functional shapes via a BV-penalty term: a gamma-convergence result*, arXiv:1503.07685 [math], (2015). arXiv:1503.07685.

[11] N. Charon, *Analysis of geometric and functionnal shapes with extension of currents. Application to registration and atlas estimation.*, PhD thesis, École Normale Supérieure de Cachan, 2013.
[12] N. Charon and A. Trouvé, *The varifold representation of nonoriented shapes for diffeomorphic registration.*, SIAM J. Imaging Sciences, 6 (2013), pp. 2547–2580.
[13] F. Chazal, D. Cohen-Steiner, A. Lieutier, and B. Thibert, *Stability of curvature measures*, CoRR, abs/0812.1390 (2008), http://arxiv.org/abs/0812.1390.
[14] D. Cohen-Steiner and J.-M. Morvan, *Restricted Delaunay Triangulations And Normal Cycle*, SoCG'03, (2003).
[15] S. Durrleman, *Statistical models of currents for measuring the variability of anatomical curves, surfaces and their evolution.*, PhD thesis, Universit Nice - Sophia Antipolis, 2010.
[16] H. Federer, *Curvature measures*, Trans. Amer. Maths. Soc., 93 (1959).
[17] H. Federer, *Geometric Measure Theory*, Springer, 1969.
[18] J. H. Fu, *Convergence of curvatures in secant approximations*, Journal of Differentiel Geometry, 37 (1991).
[19] J. H. Fu, *Curvatures Measures of Subanalytic Sets*, American Journal of Mathemtics, 116 (1994).
[20] J. Gallier, *Notes on Spherical Harmonics and Linear Representations of Lie Groups*, 2013.
[21] J. Glaunès, *Transport par difféomorphismes de points, de mesures et de courants pour la comparaison de formes et l'anatomie numérique.*, PhD thesis, Universit Paris 13, 2005.
[22] J. Glaunès, A. Qiu, M. Miller, and L. Younes, *Large deformation diffeomorphic metric curve mapping*, International Journal of Computer Vision, 80 (2008), pp. 317–336, doi:10.1007/s11263-008-0141-9.
[23] D. C. Liu and J. Nocedal, *On the limited memory BFGS method for large scale optimization*, Mathematical Programming, 45 (1989), pp. 503–528, doi:10.1007/BF01589116.
[24] C. A. Micchelli, Y. Xu, and H. Zhang, *Universal kernels*, Journal of Machine Learning Research, 7 (2006), pp. 2651–2667.
[25] M. Micheli and J. A. Glaunès, *Matrix-valued kernels for shape deformation analysis*, Geometry, Imaging and Computing, 1 (2014), pp. 57–139.
[26] M. I. Miller, A. Trouvé, and L. Younes, *Geodesic Shooting for Computational Anatomy*, Journal of Mathematical Imaging and Vision, 24 (2006), pp. 209–228.
[27] J.-M. Morvan, *generalized curvatures*, Springer, 2008.
[28] T. Rado, *What is the area of a surface?*, The American Mathematical Monthly, 50 (1943), pp. 139–141, http://www.jstor.org/stable/2302392.
[29] J. Rataj and M. Zähle, *Curvatures and currents for unions of sets with positive reach, ii*, Annals of Global Analysis and Geometry, 20, pp. 1–21, http://dx.doi.org/10.1023/A:1010624214933.
[30] US Dept of the Interior Fish and Wildlife Service, *Fishes of the gulf of maine*, 1953, http://www.nefsc.noaa.gov/lineart/.
[31] C. Thäle, *50 years sets with positive reach, a survey*, Surveys in Mathematics and its Applications, 3 (2008).
[32] M. Vaillant and J. Glaunès, *Surface Matching via Currents*, in Information Processing in Medical Imaging, G. E. Christensen and M. Sonka, eds., no. 3565 in Lecture Notes in Computer Science, Springer Berlin Heidelberg, 2005, pp. 381–392.
[33] T. Werther, *Optimal Interpolation in Semi-Hilbert Spaces*. 2003.
[34] L. Younès, *Shapes and Diffeomorphisms*, Springer, 2010.
[35] M. Zähle, *Integral and current representation of Federer's curvature measure*, Arch. Maths., 23 (1986), pp. 557–567.
[36] M. Zähle, *Curvatures and currents for unions of set with positive reach*, Geometriae Dedicata, 23 (1987), pp. 155–171.